

Article

Impact of Grain-Coating Clays on Porosity Preservation in Paleocene Turbidite Channel Sandstones: Nelson Oil Field, UK Central North Sea

Abdulwahab Muhammad Bello ^{1,*} , Stuart J. Jones ², Jon Gluyas ² and Khalid Al-Ramadan ³

¹ Centre for Integrative Petroleum Research, King Fahd University of Petroleum and Minerals, Building 78, Dhahran 31261, Saudi Arabia

² Department of Earth Sciences, Durham University, Durham DH1 3LE, UK; stuart.jones@durham.ac.uk (S.J.J.); j.g.gluyas@durham.ac.uk (J.G.)

³ Department of Geosciences, King Fahd University of Petroleum and Minerals, Building 76, Dhahran 31261, Saudi Arabia; ramadank@kfupm.edu.sa

* Correspondence: abdulwahab.bello@kfupm.edu.sa

Abstract: The Forties Sandstone Member is an important deep-water reservoir in the Central North Sea. The role of depositional characteristics, grain-coating clays, and diagenesis in controlling the reservoir quality of the sandstones is poorly understood. The main aim of the study is to understand the role of depositional characteristics, grain-coating and pore-filling clays, and diagenesis in controlling the reservoir quality evolution of turbidite-channel sandstones. The study employed a multi-disciplinary technique involving thin section petrography and scanning electron microscopy (SEM) to investigate the impact of grain size, clay matrix content, mode of occurrence of grain-coating chlorite and illite, and their impact in arresting quartz cementation and overall reservoir quality in the sandstones. Results of our study reveal that porosity evolution in the sandstones has been influenced by both primary depositional characteristics and diagenesis. Sandstones with coarser grain size and lower pore-filling clay content have the best reservoir porosity (up to 28%) compared to those with finer grain size and higher pore-filling clay content. Quartz cement volume decreases with increasing clay-coating coverage. Clay coating coverage of >40% is effective in arresting quartz cementation. Total clay volume of as low as 10% could have a deleterious impact on reservoir quality. The Forties Sandstone Member could potentially be a suitable candidate for physical and mineralogical storage of CO₂. However, because of its high proportion (>20%) of chemically unstable minerals (feldspar, carbonates, and clays), their dissolution due to CO₂ injection and storage could potentially increase reservoir permeability by an order of magnitude, thereby affecting the geomechanical and tensile strength of the sandstones. Therefore, an experimental study investigating the amount of CO₂ to be injected (and at what pressure) is required to maintain and preserve borehole integrity. The findings of our study can be applied in other reservoirs with similar depositional environments to improve their reservoir quality prediction.

Keywords: deep-water turbidites; submarine fans; clay coatings; diagenesis; reservoir quality



Citation: Bello, A.M.; Jones, S.J.; Gluyas, J.; Al-Ramadan, K. Impact of Grain-Coating Clays on Porosity Preservation in Paleocene Turbidite Channel Sandstones: Nelson Oil Field, UK Central North Sea. *Minerals* **2022**, *12*, 555. <https://doi.org/10.3390/min12050555>

Academic Editor: Dakang Zhong

Received: 25 March 2022

Accepted: 27 April 2022

Published: 29 April 2022

Publisher's Note: MDPI stays neutral with regard to jurisdictional claims in published maps and institutional affiliations.



Copyright: © 2022 by the authors. Licensee MDPI, Basel, Switzerland. This article is an open access article distributed under the terms and conditions of the Creative Commons Attribution (CC BY) license (<https://creativecommons.org/licenses/by/4.0/>).

1. Introduction

Porosity and permeability are among the most important parameters of sandstones' reservoir quality (RQ), because they determine the amount of hydrocarbons a reservoir can contain and the rate at which they can be produced, respectively [1]. RQ in sandstones is primarily controlled by two factors: (1) primary depositional parameters that include sediment composition and texture (e.g., grain size, sorting, clay content, etc.) [1–4]; and (2) diagenetic alterations during sediment burial [5–11]. While primary depositional characteristics influence original sediment composition, texture, pore-water chemistry, and early diagenesis, diagenetic alterations affect sandstones' porosity and permeability as burial

progresses [8,12]. Thus, understanding the impact of primary depositional controls and diagenetic processes is useful for RQ prediction.

RQ is a critical risk factor in exploration for hydrocarbons and carbon capture and storage [13–16]. Therefore, it is essential to understand the impact of diagenesis on RQ evolution of sandstones in order to enhance prediction of RQ away from wells [8]. Sandstones' RQ generally decreases with an increase in depth due to mechanical and chemical compaction processes, which reduce porosity and permeability [17]. Authigenic quartz overgrowth is often considered as the most significant diagenetic cement and the major control on RQ in deeply-buried, quartz-rich sandstones [18–21]. However, clay mineral coatings on sand grains are widely reported for preservation of anomalously high porosity in deeply buried sandstone reservoirs, by arresting the development of ubiquitous, porosity-occluding quartz overgrowths [22–29]. Additionally, numerous published studies have documented the formation of grain-coating clays (e.g., chlorite) in coastal sandstones, with deltaic and estuarine depositional environments being particularly common [30,31]. However, little has been published on the formation of clay coatings and the role of diagenesis in RQ evolution of deep-water sandstones deposited by sediment gravity flows. Consequently, this study aims to investigate the controls on RQ of deep-water, turbidite-channel sandstones of the Forties Sandstone Member, UK Central North Sea.

Studies on RQ evolution of deep-water turbidite sandstones are significant for two main reasons: (1) Deep-water turbidites are important hydrocarbon exploration targets, and as hydrocarbon exploration focus shifts towards more-challenging, poorly-understood deep-water sandstones, the need to include RQ in pre-drill assessment is even more important [1,28]. (2) As hydrocarbon production attains maturity stage in, for instance, almost all major oil and gas field of the axial Forties Fan system [32], the Forties Sandstone Member can be a potential site for geologic carbon capture and storage (CCS). Reservoir porosity and permeability have been identified as key controls on the efficiency and effectiveness of CO₂ injection into the subsurface geological formations for both CO₂ storage and enhanced hydrocarbon recovery. This is because low-porosity or low-permeability are often influenced by high volume of clay minerals and ductile grains, poor sorting, quartz cementation, and illite growth [16]. In this study, we documented the role of depositional characteristics and diagenesis (particularly grain-coating clays) on RQ evolution of the Forties submarine turbidite-channel sandstones in two wells from Nelson oil field, UK Central North Sea (Figure 1). The aim of the study was to answer the following questions:

What depositional characteristics have influenced RQ in these deep-water, turbidite-channel sandstones?

What role do grain-coating and pore-filling clays play in controlling the RQ?

What percentage of clay-coating coverage will significantly inhibit quartz cementation?

How does diagenesis and authigenic cements control potential CO₂ storage of turbiditic sandstone reservoirs?

1.1. Geological Setting

The Paleocene Forties Sandstone Member of the Sele Formation is a turbidite sandstone deposited in a series of overlapping submarine fans in the Central North Sea [32–34] (Figure 1). The turbidite sandstones of the Sele Formation have been divided into two major systems: (1) the primary, NW-SE-trending sediment dispersal system, which measures ca. 300 km by 100 km [32]; and (2) the E-W-trending lateral fans [32,35,36] (Figure 1). Sourced from the Outer Moray Firth, the NW-SE sediment route constitutes the axial Forties Fan, which is the main focus of this study, and forms the major reservoir to the Forties, Everest, Nelson, Montrose, Arbroath, Arran, Pierce, and Blane fields [32,37] (Figure 1). The secondary lateral fans systems were sourced from the west and serve as the main sediment source for the reservoirs in fields such as the Bittern and Gannet, and also extend as far east as Merganser and Scoter fields in the Central Graben [32] (Figure 1).

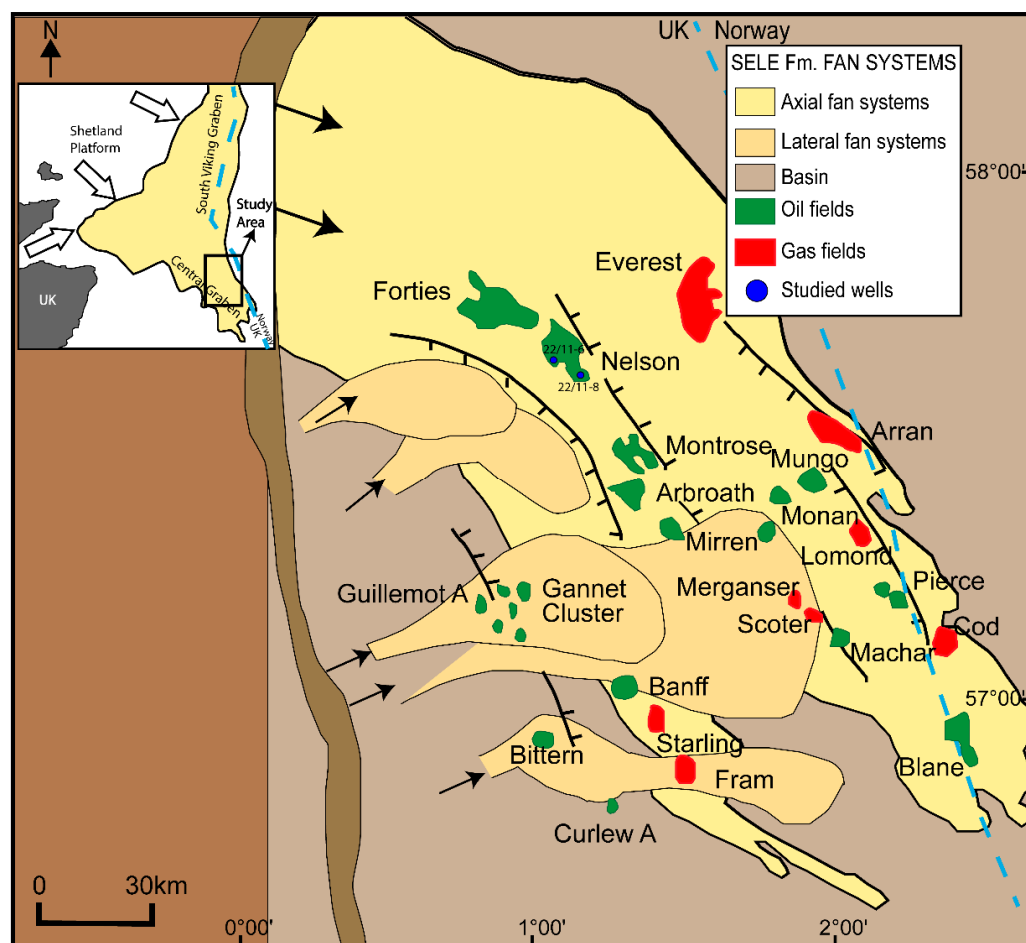


Figure 1. Regional map of the Forties Fan system showing locations of the studied wells in Nelson Field. Modified from [32]).

The early Paleocene rifting of the Greenland and European plates, which was associated with thermal doming, uplifted the Scottish Highlands up to 2 km [38], causing more than an 800 m fall in relative sea level and basinward regression [39]. This resulted in intensified erosion of the uplifted igneous, metamorphic, and meta-sedimentary hinterland, accumulating extensive deltaic and shallow marine sediments on the basin margin. Unstable delta fronts were created owing to high sedimentation rates and steep basin margins, transporting large volumes of sediments into the basin by sediment gravity flows along the major NW-SE graben axes [40]. Consequently, the Forties fan system developed as a product of the transport of accumulated clastic deltaic and shelf sediments into deep-water setting by gravity flows [33,41,42].

1.2. Stratigraphy

Ref. [43] established the lithostratigraphic framework for the Palaeogene Central North Sea, and was reviewed further using biostratigraphic techniques [34,44,45], seismic reflection data, and additional well data [46]. Based on the periods of relative sea level falls, three major depositional cycles of deep-water sedimentation have occurred in the Central North Sea during the Paleocene to early Eocene [47], and each cycle represents a period of sediments routing from the shelf to the basin floor due to the relative sea level lowstand [37]. The first depositional cycle consists of the Maureen Sandstone Member of the Maureen Formation (63–59.8 Ma) and the Lista Sandstone Member of the Lista Formation (56.8–59.8 Ma) (Figure 2), which constitute the first and second deep-water depositional cycles, respectively. The two formations have been named as the Montrose Group [48]. The Montrose Group is overlain by the Moray Group, which forms the third

depositional cycle, consisting of the Sele Formation (56.8–54 Ma) and the Balder Formation (Figure 2). The Forties Sandstone Member of the Sele Formation is a thick, discrete fan turbidite sandstone (over 200 m) and aerially extensive (ca. 300 km by 100 km) [32,46]. A regional, basinal mudstone of the Sele Formation (Figure 2) was deposited at the end of the Paleocene in response to a sea level rise. These mudstones act as regional seal for the Forties sandstone reservoirs [42]. The axial, NW-SE Forties fan (Figure 1), dominated by channels and submarine fan lobes, forms the main focus of the present study.

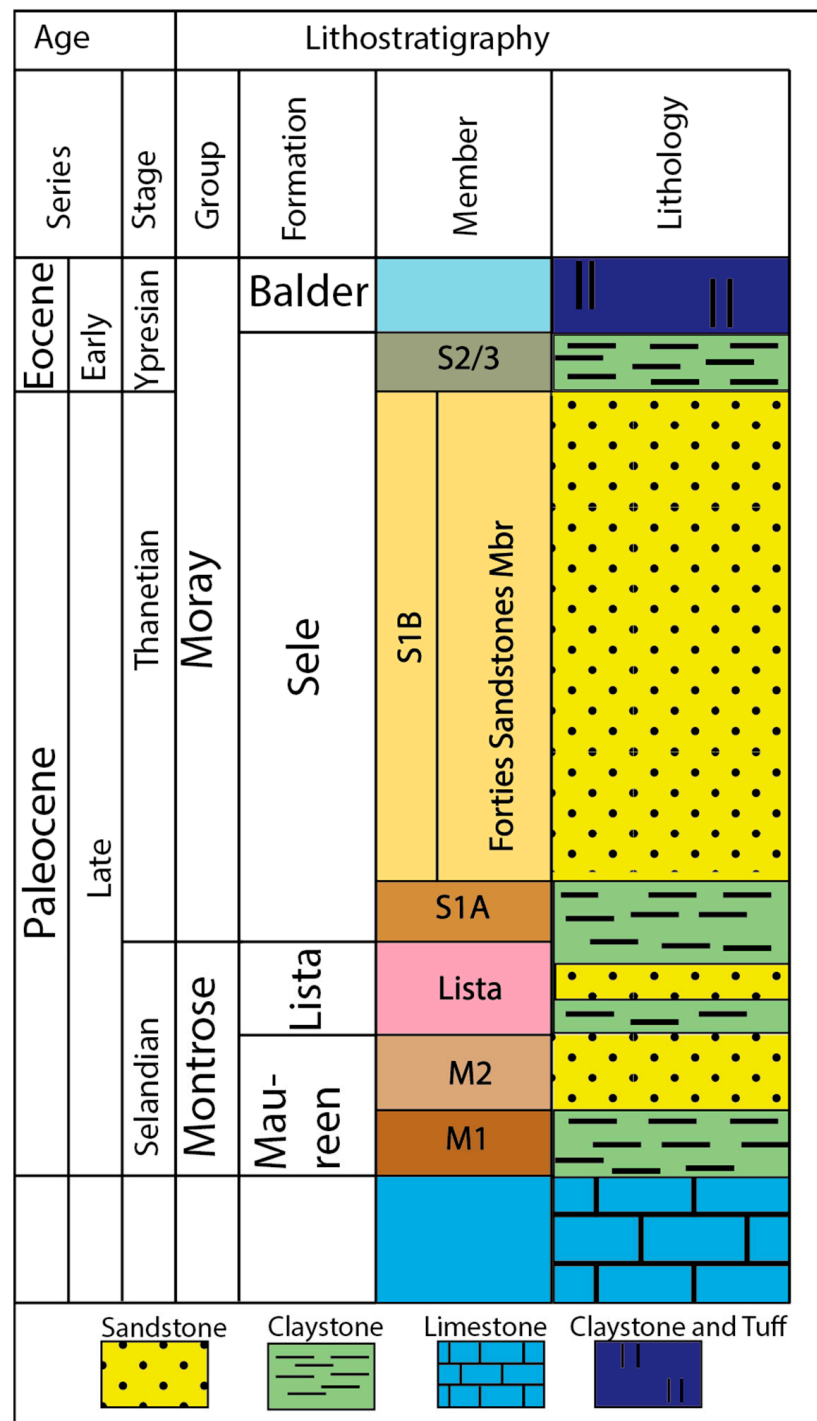


Figure 2. Stratigraphic column for the subsurface Paleocene and early Eocene formations, Central Graben, North Sea showing the studied Forties Sandstone Member of the Sele Formation.

1.3. The Nelson Field

The Nelson field is located in Blocks 22/11, 22/6a, and 22/12a in the UK Central North Sea at about 200 km east north east of Aberdeen where water depth is 88 m. The field lies between Forties field and Montrose-Arbroath fields (Figure 1). Although the first well in the field (22/11-1) was drilled in 1967, it penetrated an inter-channel area of the fan, and was not registered as an oil discovery despite oil being present in thin sandstones. However, a major discovery was made in 1988 following drilling of well 22/11-5 [42,49]. Recoverable oil reserves were estimated to be 420 million barrels, with a remaining field life of approximately 20 years (as of 2020) [49], making Nelson one of the largest oil discoveries in UK North Sea.

The field has been described as a dip-closed structure situated on Forties-Montrose High, with oil accumulations occurring in a series of submarine channel complexes of the Paleocene Forties Sandstone Member [49]. The submarine channels run in a NW-SE direction across the structure. The oil was sourced from the Jurassic Kimmeridge Clay Formation in the adjacent basins, and oil migration onto the Forties-Montrose High was interpreted to have occurred during late Miocene to early Pliocene [42]. The Balder Formation serves as the seal to the Forties reservoirs.

2. Materials and Methods

2.1. Point Count and Grain Size Analyses

Thirty-eight (38) representative sandstone core samples of the Forties Sandstone Member were collected from two wells (22/11-6 and 22/11-8; Figure 1), which penetrated a submarine channel (towards a major channel margin) (2206–2609 m true vertical depth sub-sea). Thin sections were prepared and impregnated with blue epoxy resin for identification of porosity. Additionally, the thin sections were stained with alizarin red and potassium ferrocyanide for carbonate cements identification. They were then studied using a Leica DM2500P standard petrographic microscope (Leica, Wetzlar, Germany). Point count analysis was carried out using the Petrog software package based on 300 counts per thin section. The process was repeated for all the samples to determine the average percentages of detrital grains, matrix content, pore-filling and grain-coating cements, and primary and secondary porosity. Grain size was established by measuring the long axes of at least 100 unaltered detrital grains (mostly quartz) per thin section using the Petrog software (v. 4.5.9.2, Conwy Valley Systems Limited, Conwy, UK), and mean grain size was determined for each sample.

2.2. SEM and EDS Analysis

To investigate the sandstones microstructure, clay mineral composition, morphology, and distribution, 10 polished and carbon-coated thin sections were studied using a Hitachi SU70 scanning electron microscope (SEM) (SU70, Hitachi High Technologies Corporation, Tokyo, Japan) equipped with backscatter (BSE) and an energy dispersive X-ray spectrometer (EDS). The analysis was conducted under acceleration of 12–15 kV.

2.3. Measurement of Clay-Coating Coverage

Measurements of the percentages of clay-coating coverage were conducted on 23 selected sandstone thin sections with known volumes of grain-coating chlorite, illite/illite-smectite, and quartz cement using the JMicrovision (v.1.3.3) software package based on the methodology described by [50]. The selected samples were based on high and low volumes of grain-coating clays and quartz cement determined from thin-section point counts. For each quartz grain, we measured the grain circumference, the lengths of any parts of the grain that are in contact with other grains (and hence not available for clay coatings or quartz cement to develop), and then the lengths of clay coatings on the grain surface. Clay-coating coverage was then calculated as: (sum of clay-coated lengths)/(grain circumference- sum of grain-contact lengths) [50]. The clay-coating coverage was measured on 50 quartz grains per thin section using imported, high-resolution photomicrographs into the software.

2.4. Measurements of Porosity and Permeability

Porosity and permeability (poroperm) datasets for the analysed samples were obtained from UK common data access (CDA). Porosity measurements were conducted using helium in a Boyle's Law porosimeter (Porg-200, Porg Laboratories, Tulsa, OK, USA) to give grain volume, whereas air permeability measurements were carried out using oxygen-free nitrogen as the flowing fluid with the plug mounted in a Hassler cell under a routine confining pressure of 200 psi.

2.5. Assessment of Porosity Losses from Compaction and Cementation

Assessment of compactional porosity loss (COPL) and cementational porosity loss (CEPL) was carried out following the methodology described by [51]:

$$\text{COPL} = P_i - \left[\frac{(100 - P_i)P_{mc}}{100 - P_{mc}} \right] \quad (1)$$

$$\text{CEPL} = (P_i - \text{COPL}) \left(\frac{C}{P_{mc}} \right) \quad (2)$$

where P_i is the initial or depositional porosity; P_{mc} is the intergranular volume (IGV) or minus-cement porosity, defined as the sum of detrital matrix, pore-filling cements, and intergranular porosity [52]; and C is the total pore-filling cements volume.

In the calculation of COPL and CEPL, one of the main sources of uncertainty is the initial, depositional porosity of the sandstones [53], and high estimated initial porosity would result in high compactional porosity loss. Very well- to well sorted sandstones have been reported to have initial depositional porosity of >40% [53]. Although the Forties Sandstone Member has been reported to have a depositional porosity of 36%–43% [42,54], an average, initial porosity of 40% was used in the calculation of COPL and CEPL, as the sandstones are poorly- to moderately well sorted. Additionally, samples whose detrital matrix was >10% and combined pore-filling cement volume > 40% were excluded from the calculation, because they might have been subjected to intense mechanical compaction and high grain-replacive cementation, respectively [51].

3. Results

3.1. Sandstone Composition and Fabric

The Forties sandstones are composed of poorly- to moderately well-sorted arkose and rarely subarkose and lithic arkose [55] (Figure 3), with dominant quartz (Q), feldspar (F), and minor lithic fragments (L). The overall, present-day average framework composition is $Q_{67}F_{28}L_5$.

Petrographic, point-count analysis reveals that monocrystalline quartz is the predominant detrital grain in all samples and accounts for 30%–49% (Table 1) of samples rock volumes (e.g., Figure 4A). Polycrystalline quartz ranges from 1 to 6% of the total rock volumes, and doubles up as a metamorphic rock fragment (e.g., Figure 4B). K-feldspar consists of orthoclase (1%–22%; e.g., Figure 4A) and microcline (trace to 3%; Figure 4B), which predominates over plagioclase (1%–8%). Mica consists of biotite and muscovite (Figure 4C), with biotite dominating over muscovite. Mudclast, heavy minerals, and glauconitic grains mainly occur in trace amounts to a few percent each in all studied samples. Detrital matrix mainly consists of brownish to green smectitic clays, ranging from 3 to 13% (e.g., Figure 4D). Three types of grain contacts were observed: point, long, and concavo-convex contacts (Figure 4A,B), with the long and concavo-convex contacts dominating in the sandstones.

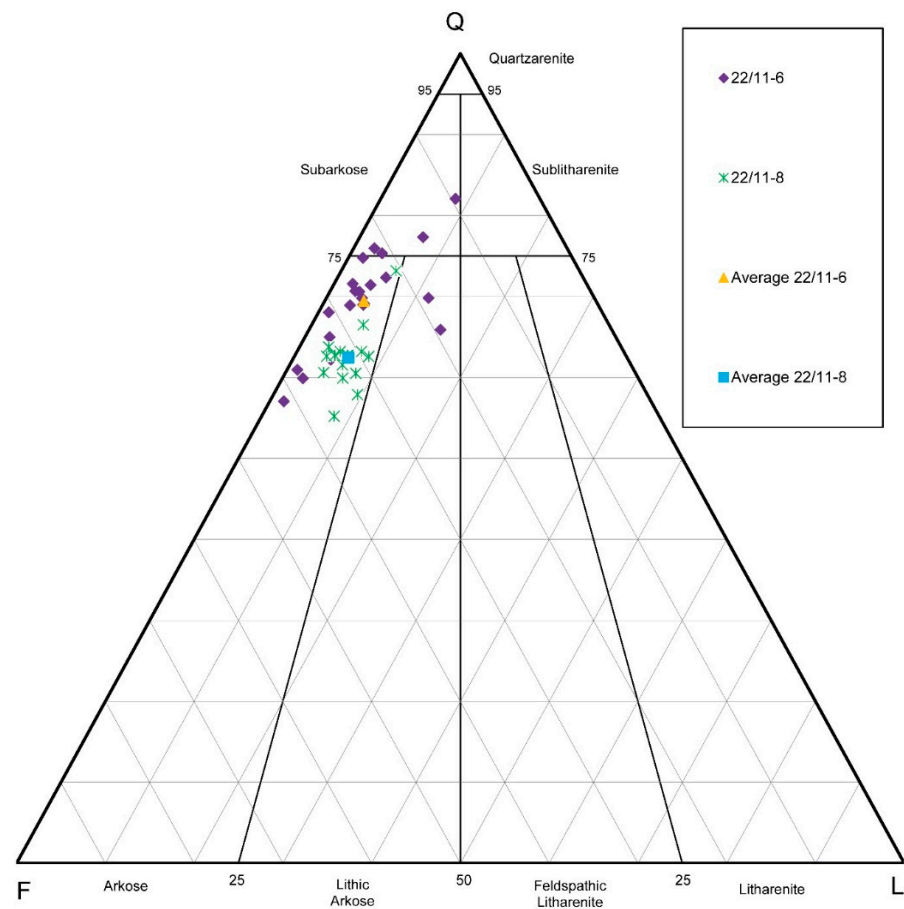


Figure 3. Modal composition for the Forties Sandstone Member, after [55,56].

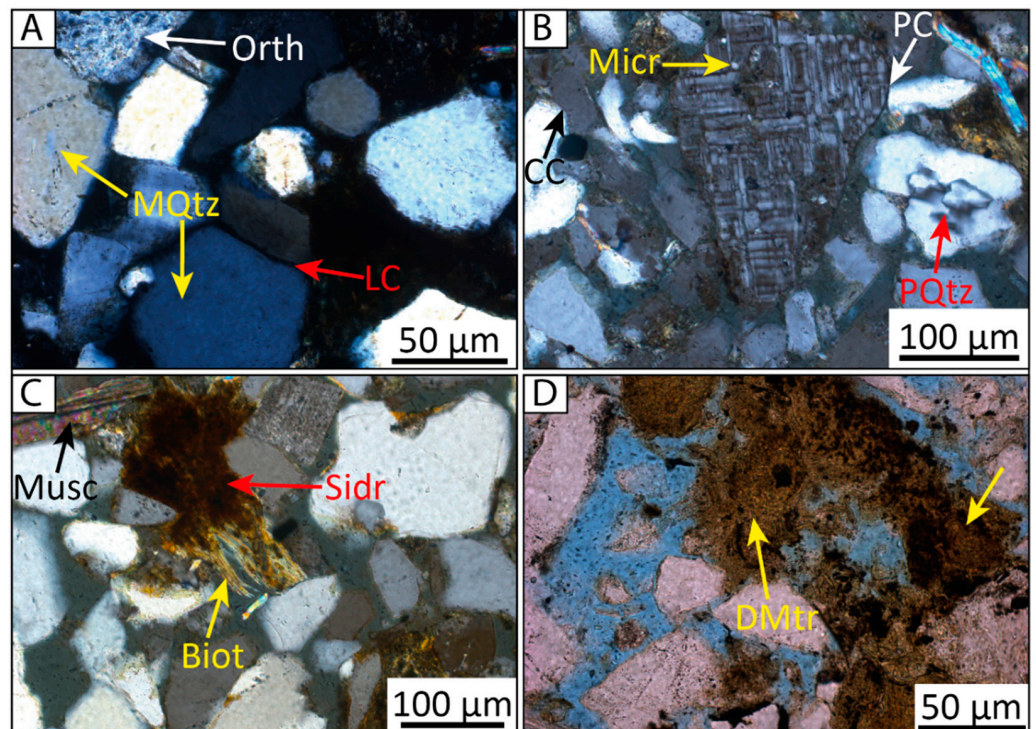


Figure 4. Thin-section photomicrographs showing detrital grains, matrix, cement, and types of grain contacts for the Forties Sandstone Member. (A) Cross-polarized-light photomicrograph showing monocrystalline quartz (MQtz), partly altered orthoclase (Orth), and long-grain contacts (LC).

(B) Cross-polarized-light photomicrograph showing microcline (Micr), polycrystalline quartz (PQtz), point contacts (PC), and concavo-convex contacts (CC). (C) Cross-polarized-light photomicrograph showing detrital muscovite (Musc), detrital biotite (Biot), and siderite (Sidr). (D) Plane-polarized-light photomicrograph showing greenish-brown, smectitic detrital matrix.

Table 1. Statistical summary of petrographic and petrophysical parameters of the Forties Sandstone Member.

Point Count and Petrophysical Data	Well 22/11-6; Number of Samples: 22			Well 22/11-8; Number of Samples: 16			All Samples; Total Number of Samples: 38		
	Min	Max	Average	Min	Max	Average	Min	Max	Average
Detrital Grains									
Monocrystalline quartz	33.30	48.70	40.79	29.70	40.00	37.26	29.70	48.70	39.31
Polycrystalline quartz (and rock fragment)	0.70	6.00	2.15	1.00	4.70	2.21	0.70	6.00	2.17
Mudclast	0.00	3.00	0.43	0.00	3.70	1.46	0.70	3.70	0.86
Total Detrital Feldspar	5.30	26.10	15.48	11.00	22.00	18.80	5.30	26.10	16.88
Orthoclase	1.30	21.70	11.11	5.70	15.70	12.43	1.30	21.70	11.67
Microcline	0.00	2.70	0.86	0.00	1.00	0.19	0.00	2.70	0.58
Plagioclase	1.00	7.70	3.50	3.70	8.30	6.19	1.00	8.30	4.63
Total rock fragments	0.70	9.00	2.58	2.00	6.00	3.66	0.70	9.00	3.03
Total mica	0.00	2.70	0.79	0.7	10.40	2.75	0.00	10.40	1.61
Biotite	0.00	1.30	0.32	0.70	4.70	1.54	0.00	4.70	0.83
Muscovite	0.00	2.00	0.46	0.00	5.70	1.21	0.00	5.70	0.78
Glauconite	0.00	0.30	0.07	0.00	0.30	0.02	0.00	0.30	0.05
Heavy minerals	0.00	0.70	0.07	0.00	0.30	0.04	0.00	0.70	0.06
Detrital matrix	3.30	12.70	7.17	3.00	11.70	6.15	3.00	12.70	6.74
Diagenetic minerals									
Intergranular non-ferroan calcite	0.30	5.30	0.50	0.00	1.30	0.24	0.00	5.30	0.39
Grain-replacive non-ferroan calcite	0.00	3.00	0.14	0.00	0.70	0.16	0.00	3.00	0.14
Intergranular ferroan calcite	0.00	1.00	0.05	0.00	0.30	0.02	0.00	1.00	0.03
Grain-replacive ferroan calcite	0.00	2.30	0.22	0.00	0.17	0.12	0.00	2.30	0.18
Intergranular dolomite	0.00	7.70	0.49	0.00	1.70	0.13	0.00	7.70	0.33
Grain-replacive dolomite	0.00	0.30	0.01	0.00	0.00	0.00	0.00	0.30	0.01
Intergranular siderite	0.00	3.70	1.59	0.00	1.70	0.39	0.00	3.70	1.09
Grain-replacive siderite	0.00	1.30	0.06	0.00	0.00	0.00	0.00	1.30	0.03
Intergranular pyrite	0.00	1.30	0.55	0.00	2.00	0.39	0.00	2.00	0.48
Grain-replacive pyrite	0.00	0.70	0.11	0.00	1.00	0.26	0.00	1.00	0.17
Intergranular kaolinite	0.00	6.30	1.53	0.00	2.70	1.26	0.00	6.30	1.42
Grain-replacive kaolinite	0.00	1.30	0.14	0.00	0.70	0.16	0.00	1.30	0.15
Intergranular chlorite	0.00	4.00	1.65	1.30	5.00	2.49	0.00	5.00	2.01
Grain-replacive chlorite	0.00	1.30	0.50	0.00	1.00	0.73	0.00	1.30	0.59
Grain-coating chlorite	0.00	1.00	0.10	1.70	7.70	3.95	0.00	7.70	1.72
Intergranular illite/smectite	0.00	0.30	0.03	0.00	0.00	0.00	0.00	0.30	0.02
Grain-replacive illite/smectite	0.00	0.00	0.00	0.00	0.00	0.00	0.00	0.00	0.00
Grain-coating illite/illite-smectite	1.30	5.30	3.20	0.70	2.70	1.10	0.30	5.30	2.32
Intergranular illite	0.70	4.30	2.66	0.00	2.00	0.89	0.00	4.30	1.92
Grain-replacive illite	0.00	2.00	0.65	0.00	1.30	0.49	0.00	2.00	0.59
Quartz overgrowth	1.30	6.30	3.30	2.30	6.00	4.03	1.00	6.30	3.62
Bitumen	0.00	1.70	0.50	0.00	1.70	0.61	0.00	1.70	0.54

Table 1. Cont.

Point Count and Petrophysical Data	Well 22/11-6; Number of Samples: 22			Well 22/11-8; Number of Samples: 16			All Samples; Total Number of Samples: 38		
	Min	Max	Average	Min	Max	Average	Min	Max	Average
Porosity									
Intergranular optical porosity	7.30	18.80	12.70	0.70	17.30	9.68	0.70	18.80	11.43
Clay-lined intergranular optical porosity	0.00	4.70	0.95	0.30	5.70	2.85	0.00	5.70	1.75
Total optical porosity	7.60	20.70	13.66	1.70	20.60	12.53	1.70	20.70	13.18
Feldspar dissolution porosity	0.00	3.00	1.10	0.30	1.70	1.17	0.00	3.00	1.13
Clay-lined feldspar dissolution porosity	0.00	1.30	0.26	0.00	0.70	0.14	0.00	1.30	0.21
Total Feldspar dissolution porosity	0.00	4.00	1.36	0.30	2.40	1.31	0.00	4.00	1.34
Cements									
Cements (pore-filling) total	7.30	24.30	12.60	5.30	14.00	9.84	5.30	24.30	11.30
Carbonate cements (pore-filling) total	0.00	14.70	2.62	0.00	2.00	0.78	0.00	14.70	1.84
Authigenic, pore filling clay minerals total	3.70	9.60	5.87	1.60	8.00	4.65	1.60	9.60	5.36
Additional data									
Compactional porosity loss (%) COPL	3.23	19.79	9.98	4.45	24.15	15.76	3.23	24.15	12.41
Cementational porosity loss (%) CEPL	5.86	22.64	11.18	4.30	11.67	8.32	4.28	22.64	9.98
Intergranular volume (IGV)	25.20	38.00	33.19	20.90	37.20	28.53	20.90	38.00	31.23
Helium porosity (%)	20.30	28.40	24.30	20.10	25.00	23.70	20.10	28.40	23.86
Vertical permeability (mD)	25.00	500.00	212.68	7.10	412.00	158.80	7.10	500.00	190.00
Mean grain size (mm)	0.18	0.36	0.29	0.12	0.29	0.25	0.12	0.36	0.27

3.2. Sedimentological Description and Interpretation

Sedimentary logs were constructed for the two studied wells from the Nelson field (22/11-6 and 22/11-8) based on six depositional facies (Figure 5). The sedimentary facies include structureless sandstones (Sm), sandstones with water escape structures (Sw), parallel laminated (Sp) sandstones, slumped sandstones and mudstones (Sl), laminated mudstones (Ml), and hemipelagic mudstones (Mh) (Figure 6A–F). Summary of the different facies and interpretations of the depositional processes and environment are presented in Table 2. The sedimentary logs are characterized by thick, amalgamated sandstones, consisting of Sm, Sw, and Sp facies (Figure 6A–C). The amalgamated beds are commonly recognized by change in grain size, minor scour surfaces, and occasional presence of rip-up mudclasts in the basal sections of the sandstones. Individual bed thicknesses range from 20 to 100 cm. The amalgamated beds are capped by low-energy and suspension mudstone deposits (i.e., facies Ml and Mh; Figure 6F).

3.2.1. Clean, Structureless Sandstones (Sm)

These facies consist of clean, fine- to medium-grained sandstones, which lack sedimentary structures (Figure 6A). The facies may contain pebbles or mudclasts, and occasionally passes upward into sandstones characterized by water escape structures (Sw). Beds and tops are commonly sharp or undulating, with individual beds measuring several feet thick and commonly amalgamated.

The absence of sedimentary structures and the presence of amalgamation features suggest rapid deposition of sand from high-density turbidity currents confined in submarine channels [56,57].

3.2.2. Sandstones with Water Escape Structures (Sw)

These facies consist of fine- to medium-grained sandstones, which commonly form beds up to 2 m thick. Beds are generally amalgamated, with commonly sharp bed contacts.

The facies are closely associated with Sm and Sp. The sedimentary structures consist of water escape pipes (p) and dish structures (d) (Figure 6B,C).

These sandstones are interpreted as products of high-density turbidity current, which have undergone sediment dewatering during or shortly after deposition [17,56].

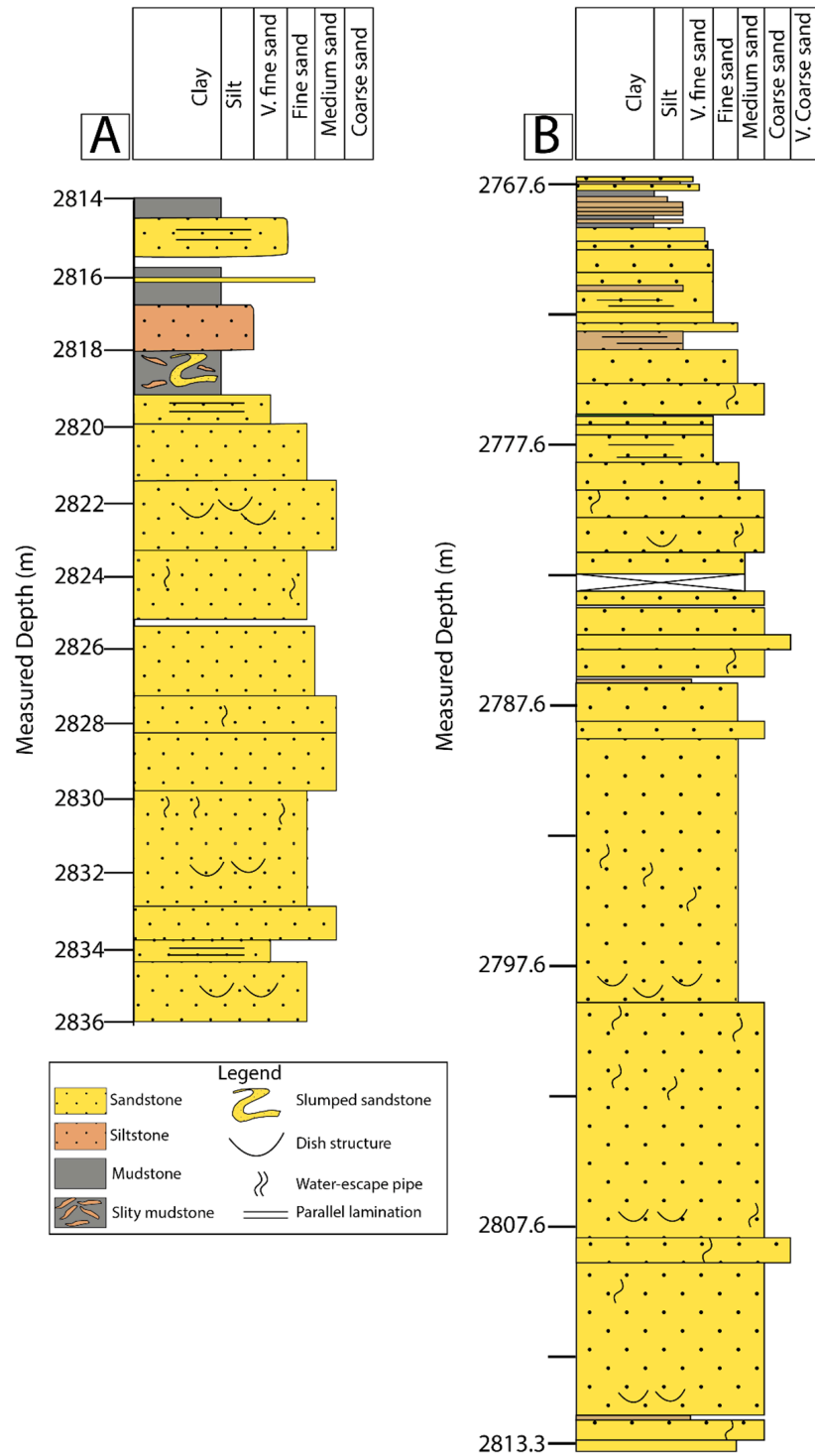


Figure 5. Representative sections of the sedimentary core logs for the Forties Sandstone Member in (A) 22/11-6 and (B) 22/11-8.

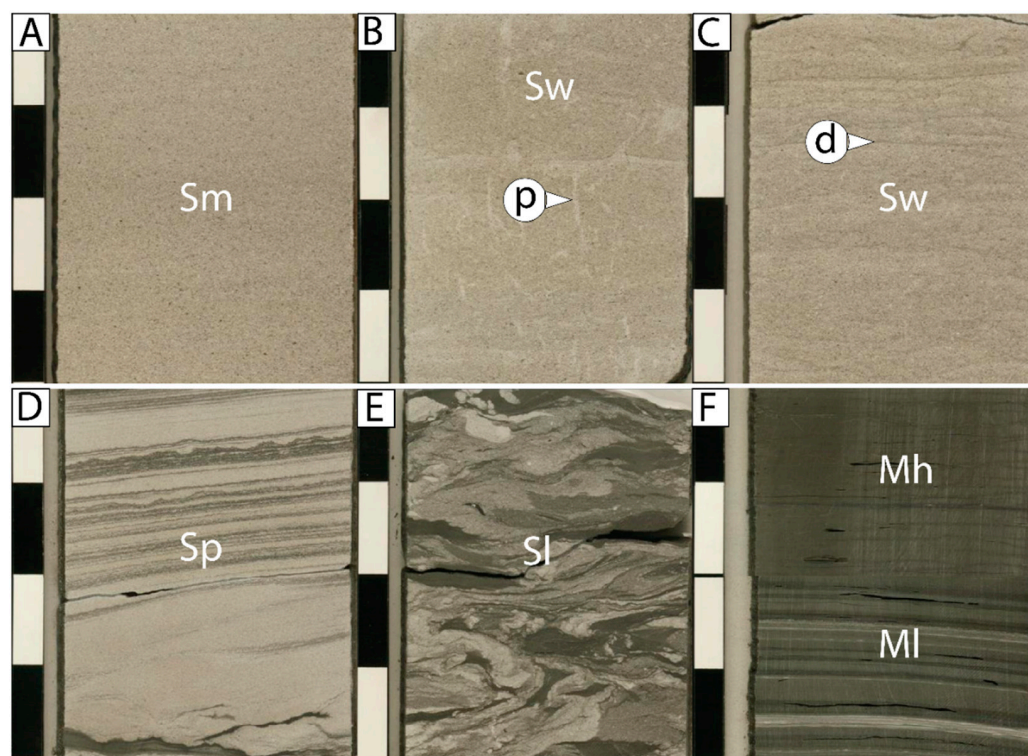


Figure 6. Core photographs of sedimentary facies for the Forties Sandstone Member. (A) Clean, structureless sandstones (Sm). (B) Sandstone with water-escape pipes (p). (C) Sandstone with dish structures (d). (D) Parallel-laminated sandstones (Sp). (E) Slumped sandstone and mudstone (Sl). (F) Laminated mudstone (MI) and hemipelagic mudstone (Mh). Note that the black and white scale bars = 3 cm each.

Table 2. Classification, description, and interpretation of sedimentary facies for the Forties sandstones.

Facies		Bed Thickness (cm)	Figure	Textures and Sedimentary Structures	Interpretation	
Code	Description				Process	Depositional Environment
Sm	Clean, structureless sandstones	50–100	Figure 6A	Fine- to medium grained, poorly- to moderately well-sorted, structureless, with occasional mudclasts	High-density turbidity currents	Probable submarine channel
Sw	Sandstones with water escape structures	20–30	Figure 6B,C	Fine- to medium-grained, poorly- to moderately well-sorted, with dish and pipe structures	High-density turbidity currents	Probable submarine channel
Sp	Parallel laminated sandstones	20–30	Figure 6D	Fine grained, poorly sorted	High-density turbidity currents	Probable submarine channel
Sl	Slumped sandstones and mudstones	20–60	Figure 6E	Very fine- to fine-grained, generally poorly sorted sandstones. They are characterized by gradational to sharp bases and tops	Local oversteepening or loading at bed contacts	submarine channel
MI	Laminated mudstones	5–10	Figure 6F	Fissile mudstone/shale with variable silt content	Dilute low-density turbidites and suspension deposits	Distal fan and interchannel
Mh	Hemipelagic mudstones	10–20	Figure 6F	Greenish grey mudstones, rare sand injections	Suspension deposits	Channel margin/abandonment, interchannel, basinal mudstone

3.2.3. Parallel Laminated Sandstones (Sp)

These sandstones are mainly fine- but locally medium-grained. The sandstones are characterised by faint, parallel laminae, defined by variation in grain size (Figure 6D). Beds are commonly amalgamated and characterized by sharp tops and bases. Additionally, the laminated intervals are closely associated with Sm and Sd facies in the same depositional unit.

These facies are interpreted to have been deposited by dilute, slightly unstable but fully turbulent high-density turbidity current [57].

3.2.4. Slumped Sandstones and Mudstones (Sl)

Slumped facies are deformed, minor component in the cored interval, which lack internal sedimentary structures (Figure 6E). They occur locally in facies Sw, often less than 1 m, and are characterized by gradational to sharp bases and tops.

The thin, slumped units record soft sediment deformation that can be attributed to local oversteepening (e.g., salt-induced highs) or loading at bed contacts [56,58].

3.2.5. Laminated Mudstones (Ml)

These facies represent the top of the Forties sandstones and generally occur as thin bed (<30 cm). It has variable silt content and occasionally contain thin sandstone laminae (Figure 6F). They generally occur as thin bed (<30 cm).

The mudstone/shale facies are interpreted to represent the deposition from suspension by both background marine hemipelagic sedimentation and dilute muddy and silty low-density turbidites [59]. The thin sandstones laminae within the mudstones/shales represent thin, distal 'classical' turbidites. Overall, these sediments probably represent interchannel and channel margin depositional environments.

3.2.6. Hemipelagic Mudstones (Mh)

These facies consist of massive greenish to grey mudstones (Figure 6F), with occasional sand injections. Bed tops and bases are sharp and often gradational. The facies have been interpreted as a product of hemipelagic suspension fallout [59].

3.3. Diagenetic Minerals

The diagenetic minerals include authigenic clays, carbonate cements, and quartz overgrowths, representing the principal diagenetic mineral phases encountered in the studied sandstones.

3.3.1. Clay Minerals

Kaolinite (trace to 6%) occurs in both primary intergranular and secondary feldspar-or mica-dissolution pores (Figure 7A,B). It is represented by vermicular pattern or patches of 'booklets' of pseudo-hexagonal platelets, within which microporosity is preserved. Kaolinite replaces dissolved feldspar or mica grain (Figure 7B). Occasionally, kaolinite transforms into its blocky, higher-temperature form (dickite) (Figure 7A). Pore-filling kaolinite and dickite significantly reduce intergranular porosity where they are well developed (Figure 7A). Kaolinite has been observed to engulf pyrite (Figure 7B)

Chlorite occurs as both grain-coating and pore-filling clay (Figure 7C,D). Grain-coating chlorite (trace to 8%) occurs as rims around quartz and other detrital grains (Figure 7C), whereas pore-filling chlorite occurs as crystal aggregates within intergranular pores (Figure 7D). Additionally, like kaolinite, chlorite replaces mica grains (e.g., biotite; Figure 7B).

Authigenic illite is present as fibrous, hair-like crystal aggregates, occurring as grain-coating and pore-filling clay (Figure 7B,E,F). SEM analysis has revealed that illite commonly occurs in close association with mixed-layer illite-smectite. Grain-coating illite in the studied sandstones ranges from trace to 5%, whereas pore-filling illite ranges from trace to

4%. Furthermore, illite replaces authigenic kaolinite, bridging pore throats and occluding intergranular porosity (Figure 7F).

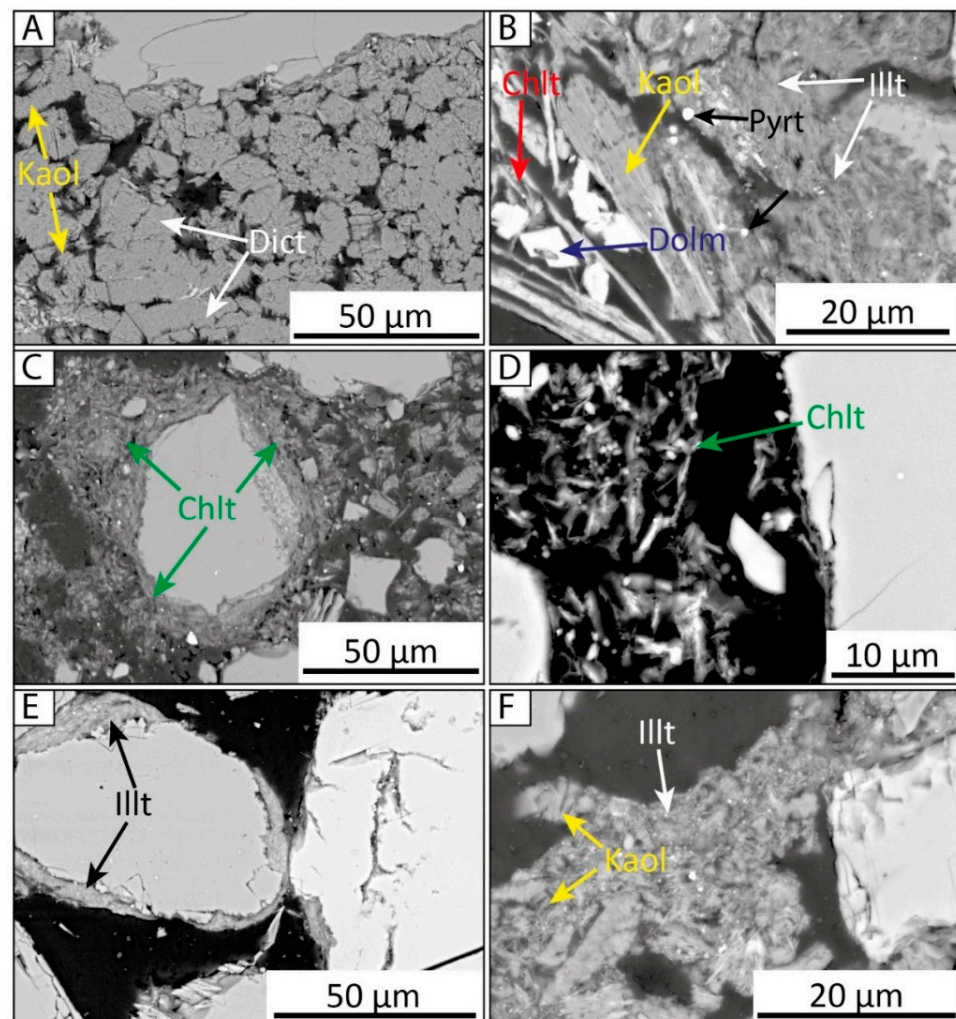


Figure 7. BSE images of the Forties Sandstone Member depicting clay types and mode of occurrence. (A) Pore-filling kaolinite (Kaol) transforming into blocky, higher-temperature polymorph (dickite; Dict). (B) Fibrous, pore-filling illite destroying intergranular porosity. (C) Formation of thick grain-coating chlorite and its transformation into pore-filling chlorite. (D) Pore-filling chlorite reducing intergranular porosity. (E) Grain-coating illite preventing the formation of quartz overgrowths. (F) Pore-filling illite replacing kaolinite and destroying RQ by pore bridging and occlusion. [BSE = Backscattered Electron].

3.3.2. Carbonate Cements

The carbonate cements in the Forties sandstones consist of calcite, dolomite, and siderite. (Figures 7B and 8A–D). Calcite occurs as both ferroan and non-ferroan cements (e.g., Figure 8A–C), occluding intergranular pores. Non-ferroan calcite occurs as patchy and blocky, poikilotopic cement (Figure 8A), and occasionally shows evidence of dissolution (Figure 8C). Ferroan occurs as replacement of dissolved non-ferroan calcite and etched feldspar grains, occluding both primary and secondary pores, respectively (e.g., Figure 8C). The ferroan calcite commonly engulfs, thus postdates, feldspar (albite) and quartz overgrowths (e.g., Figure 8B). Dolomite occurs locally as rhombs within primary pores, and as replacement of altered mica grains (Figure 7B). Siderite principally occurs as scattered rhombs in loosely packed sandstones, and in the vicinity of partly-dissolved

mica grains (Figures 4C and 8D). The siderite cement often undergoes dissolution, creating interconnected primary pores in the sandstones.

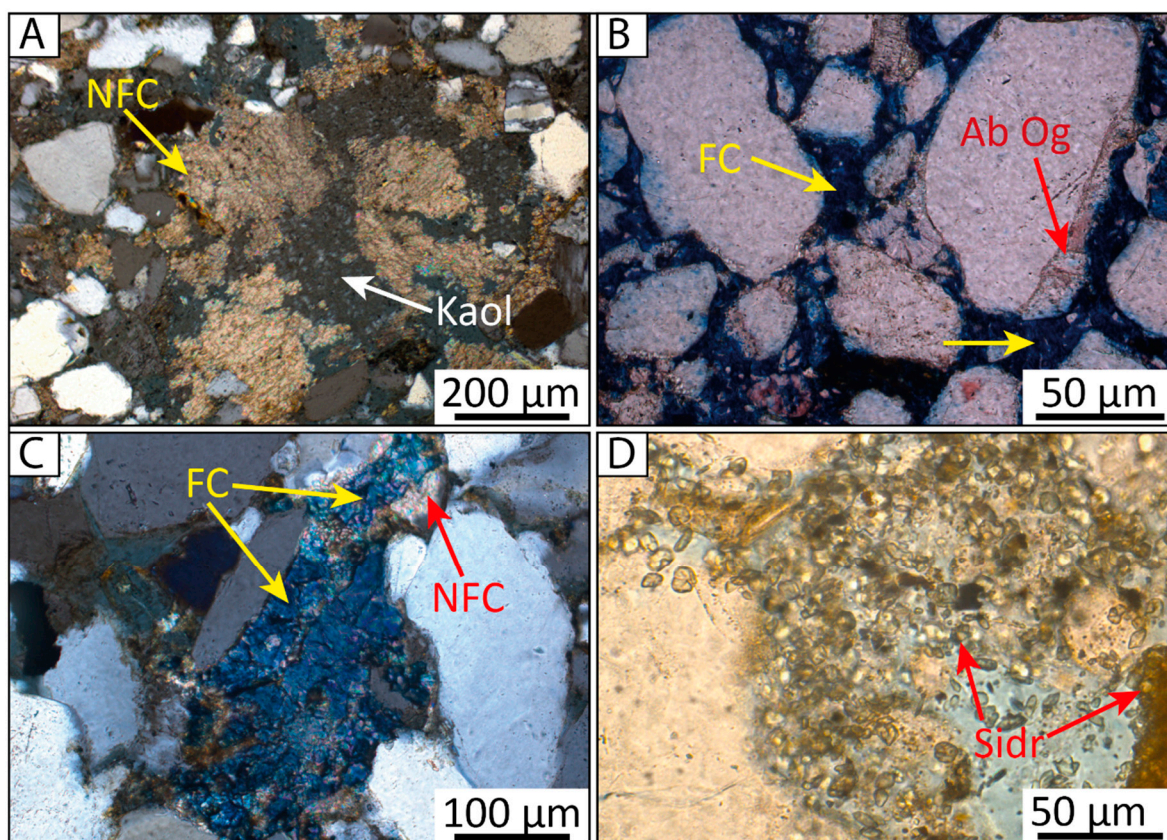


Figure 8. Thin-section photomicrographs showing the types and mode of occurrence of carbonate cements. (A) Non-ferroan calcite (NFC) filling intergranular porosity and engulfing kaolinite (Kaol). (B) Ferroan calcite (FC) and albite (Ab) overgrowth (Og) destroying intergranular porosity. (C) Ferroan calcite (FC) replacing dissolved non-ferroan calcite and filling intergranular pore space. (D) Siderite (Sidr) destroying intergranular porosity.

3.3.3. Quartz Overgrowths

Quartz cement (1%–6%) occurs as syntaxial overgrowths on detrital quartz grains (Figure 9A,B). They are identified by their smooth crystal faces, dust rim, and thin clay coats, making their contact with the host detrital grain. Quartz overgrowths grow into intergranular pores, and are often more abundant on quartz grains that lack clay coatings (e.g., Figure 9A) or where clay coatings are discontinuous (e.g., Figure 9B) or too thin.

3.3.4. Pyrite

Pyrite (trace to 2%) occurs mainly as framboids, which fills intergranular pores (Figure 9C) or replaces partly or completely dissolved feldspar or mica grains (e.g., Figure 9D). Additionally, grain-replacive pyrite occurs in close proximity to siderite or dolomite in altered mica.

3.4. Reservoir Properties

Results of the measurements of core porosity and permeability on the Forties sandstones show that the helium, core porosity ranges from 20 to 28% (av. 24%), whereas vertical permeability ranges from 7 to 500 mD (av. 190). Additionally, a plot of core porosity against permeability (Figure 10) shows a positive correlation and, in general, samples from 22/11-6 have higher porosity and permeability values than those from 22/11-8.

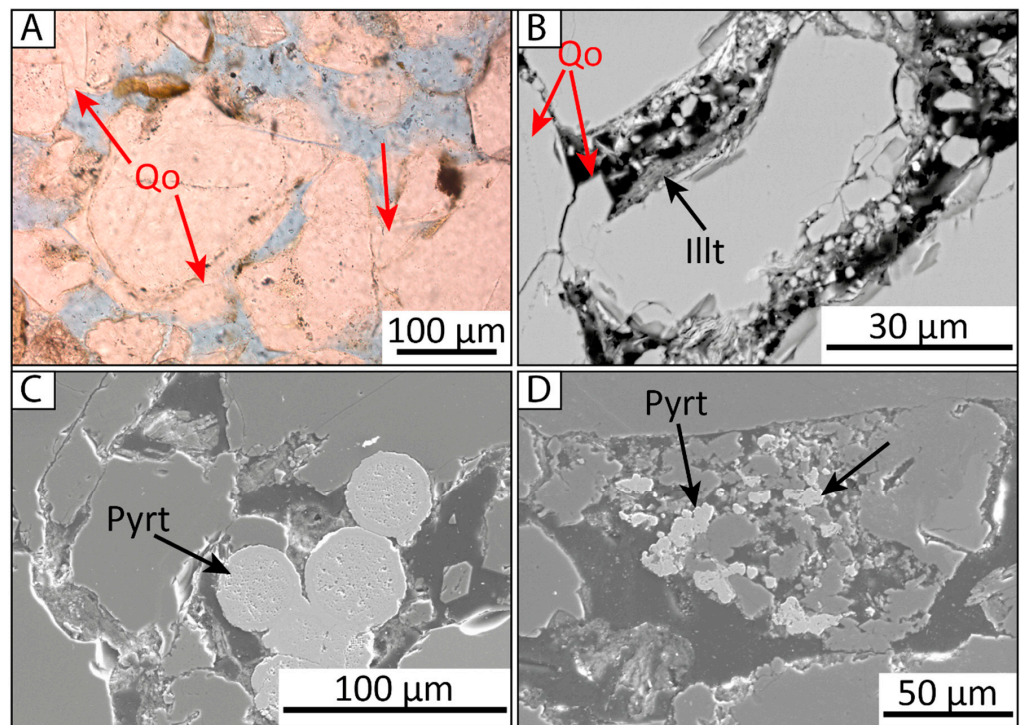


Figure 9. Thin-section, BSE, and SEM images showing the development of quartz overgrowths and the mode of occurrence of pyrite. (A) Well development of quartz overgrowths (Qo) due to lack of grain-coating clays. (B) Grain-coating illite (Illt) inhibiting the formation of quartz overgrowth (Qo). (C) Framboidal pyrite (Pyrt) filling intergranular porosity. (D) Formation of grain-replacive pyrite (Pyrt) replacing partly dissolved plagioclase feldspar. [BSE = Backscattered Electron; SEM = Scanning Electron Microscope].

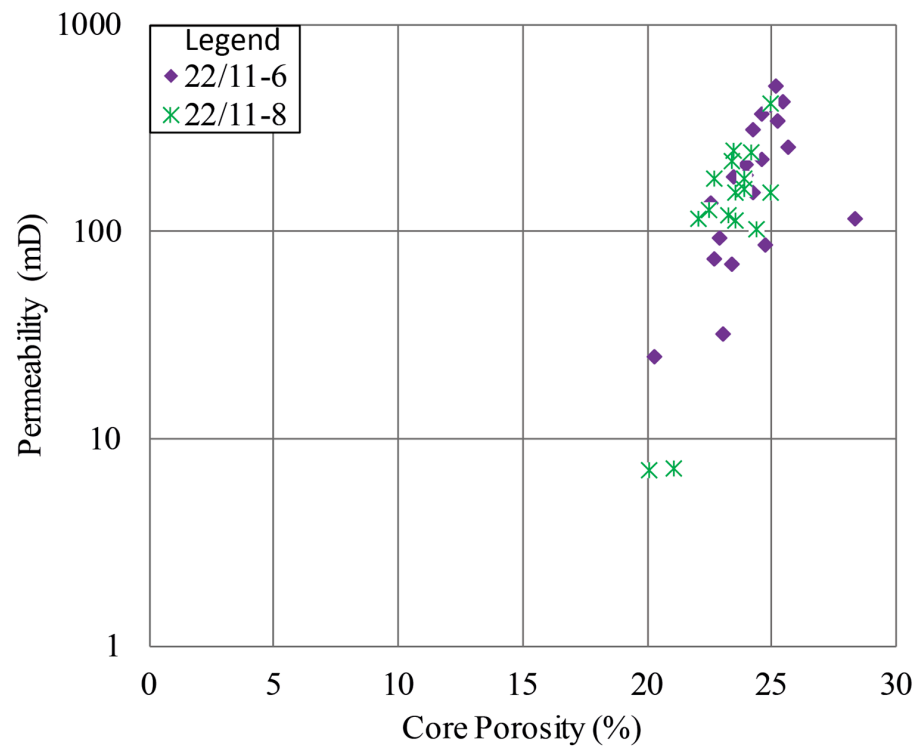


Figure 10. Reservoir porosity and permeability data for the Forties Sandstone Member. The data shows a positive correlation between the two parameters.

Furthermore, petrographic observations and SEM analysis of thin-section samples revealed two types of porosity: primary (intergranular) and secondary (intragranular) porosities. Point count data indicates that the primary, optical porosity ranges from 1 to 19% (av. 11%). Secondary intragranular, feldspar-dissolution porosity ranges from 0 to 4% (av. 1.34%).

Plots of porosity and permeability against grain size show that both increase with an increase in grain size (Figure 11A,B). However, plots of porosity and permeability against pore-filling clays indicate that the clays have a negative impact on reservoir porosity and permeability (Figure 11C,D). In addition, results of the plots of total pore-filling cements (clays+carbonates) against porosity and permeability (Figure 11E,F) indicate that high pore-filling cements have negative impacts on reservoir porosity and permeability.

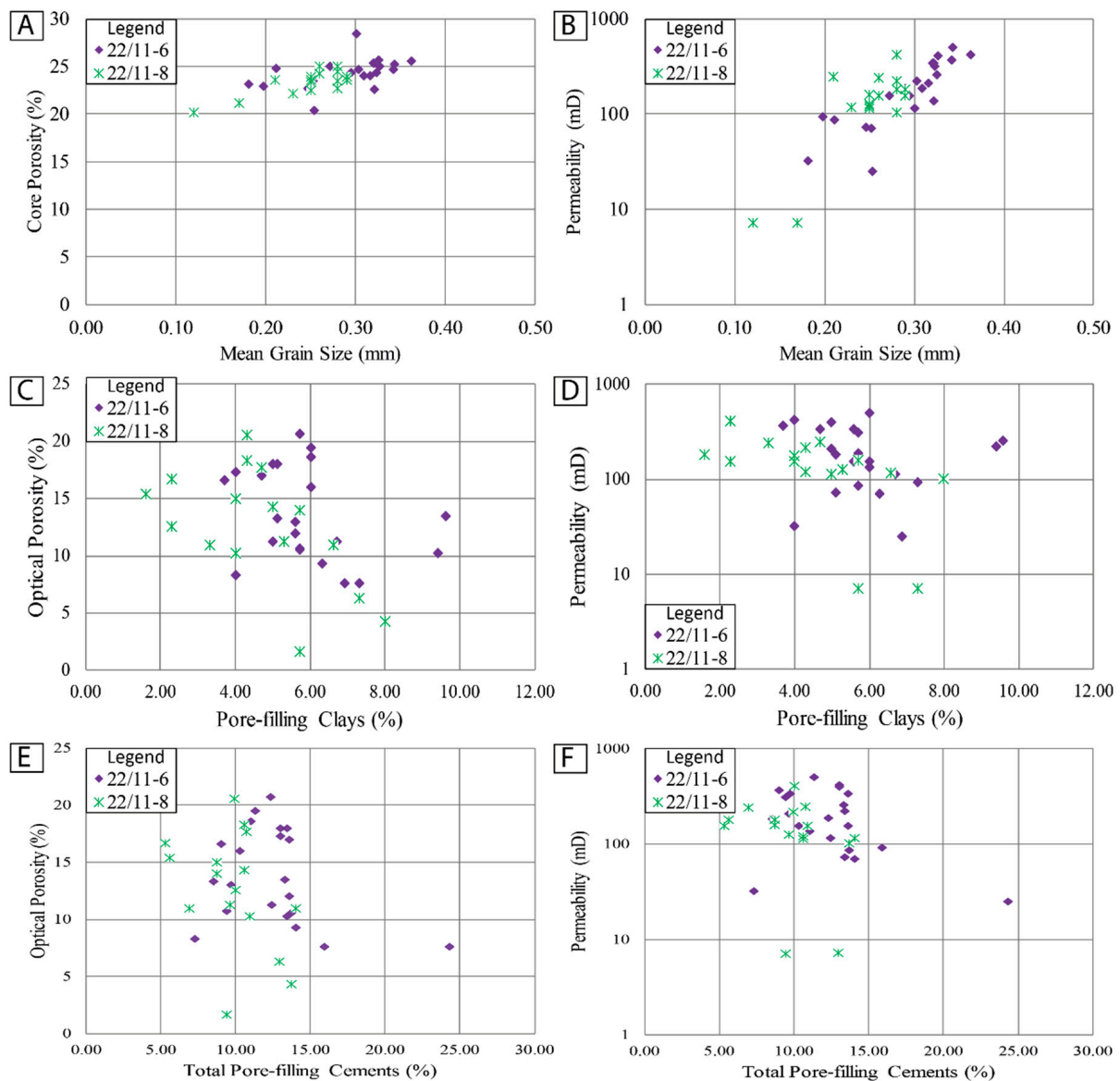


Figure 11. Impact of depositional characteristics (e.g., grain size), pore-filling clays, and cements on reservoir properties of the Forties Sandstone Member. (A,B) plots of porosity against grain size and permeability against grain size, respectively. (C,D) plots of porosity against pore-filling (authigenic) clays and permeability against pore-filling (authigenic) clays, respectively. (E,F) plots of porosity against total pore-filling cements and permeability against total pore-filling cement, respectively.

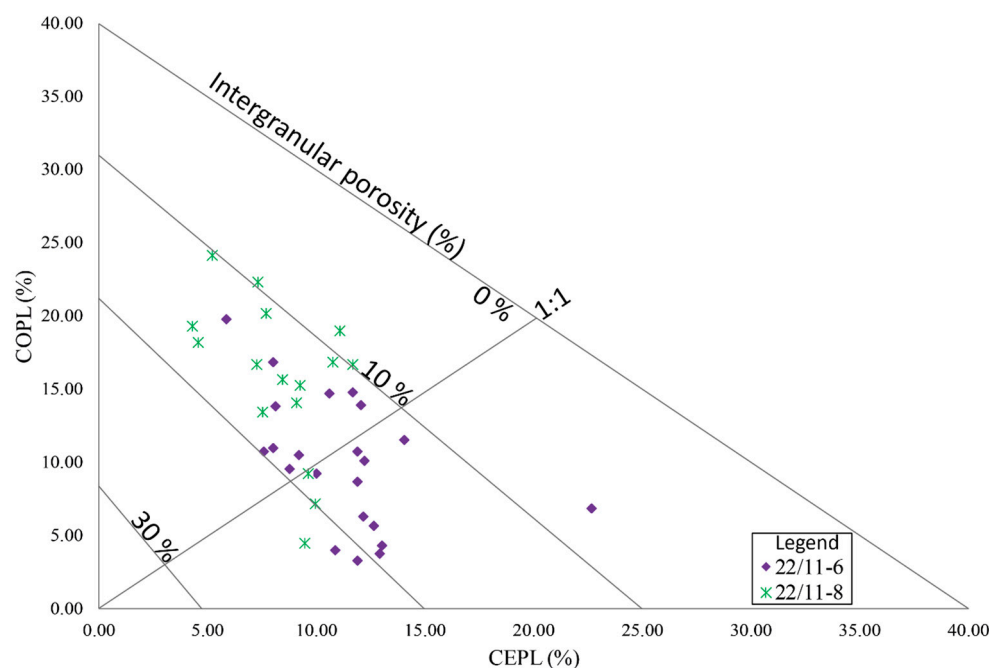


Figure 13. Plot of compactional porosity loss (COPL) against cementational porosity loss (CEPL) showing that porosity is mainly lost due to compaction than due to cementation.

Quartz overgrowths are absent where siderite and non-ferroan calcite cover quartz grain surfaces and have been observed to engulf authigenic kaolinite, suggesting that the quartz cement postdates these minerals. Dissolution of feldspar grains and clay minerals reactions (e.g., illitization of smectite) are believed to have supplied the silica required for the formation of quartz cement.

Grain-coating smectitic clays were observed at grain contacts, suggesting that they formed during early diagenesis and predated mechanical compaction. SEM-EDS analysis has revealed that grain-coating chlorite and illite were formed from smectite.

Ferroan calcite has been observed to engulf quartz cement and albite overgrowths (e.g., Figure 8B), and occurs where non-ferroan calcite has dissolved (Figure 8C), implying that the cement was formed during late diagenesis. Moreover, results of carbon and oxygen data for ferroan calcite from Forties sandstones have shown that the cements were primarily sourced from decarboxylation influenced by heat-conducting diapirs and migration of overpressured fluid from Jurassic reservoirs through faults created by the diapirs [29,66].

Clay-Coating Coverage and Quartz Cementation

Quartz overgrowths are one of the major porosity-occluding cements in deeply buried sandstone reservoirs. The formation of quartz cement depends on the availability and extent of nucleation area for quartz cementation, the temperature history of the sandstones, and the presence dissolved silica [18–21,67]. Thus, understanding the processes of formation of quartz cement is crucial for successful prediction of porosity in quartz-rich sandstones exposed to high-temperature diagenesis [17]. Clean, clay-free sandstones are susceptible to intense quartz cementation during burial [6,8,28,31], thereby destroying intergranular porosity. In contrast, sandstones with clay coatings can preserve anomalously high porosity during deep burial by preventing quartz cementation. The effectiveness of clay coatings in arresting quartz cementation depends on the coatings' thickness, mineralogy, and extent of coverage [25,27].

Our study demonstrates that thick chlorite and illite/illite-smectite coatings have inhibited the development of quartz cement in the channelized deep-water Forties sandstones, and that there is a negative correlation between quartz cement and clay-coating coverage (Figure 14A). The volume of quartz cement appears to significantly reduce when

the clay-coating coverage exceeds 40% (Figure 14A). In addition, high porosity and permeability are recorded where the clay-coating coverage is more than 40% (Figure 14B,C). The Forties Sandstone Member samples are from relatively shallow depths (2.2 to 2.6 km), and the volumes of quartz cement are generally less than 6%, thereby not significantly reducing RQ. However, well-developed quartz cements on detrital quartz grains were observed in the deepest Forties samples with thin, discontinuous or poorly-developed clay coatings (e.g., Figure 9A,B), suggesting that larger quartz cement volume and correspondingly lower porosity values would have developed if clay coatings had not coated quartz grains. Additionally, the presence of feldspar dissolution pores and the transformation of smectite to illite suggest the presence of silica in the system, but it has been largely prevented from precipitating as quartz cement by clay coatings. Thus, being able to predict the origin, type, and method of emplacement of grain-coating clays is essential for improving the prospectivity of deep-water reservoirs.

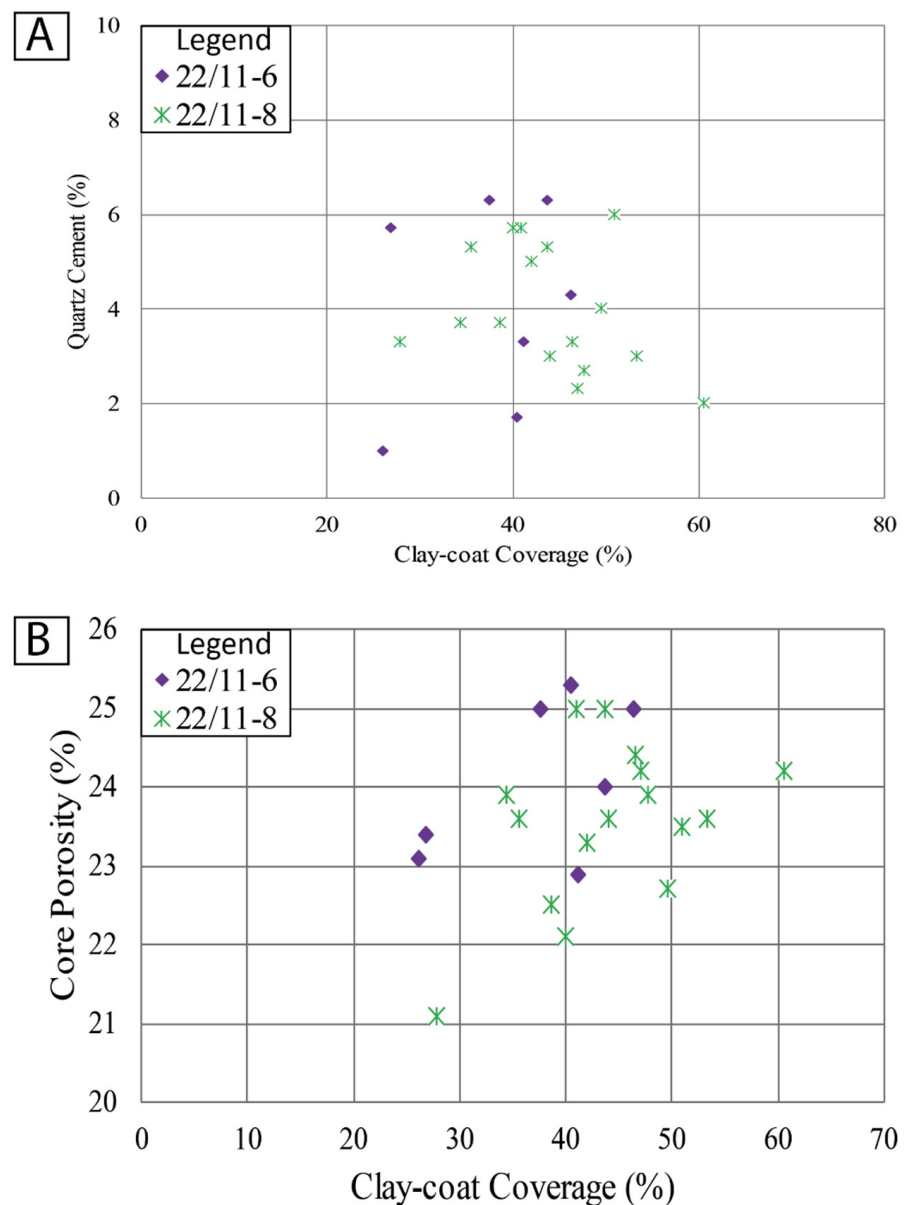


Figure 14. Cont.

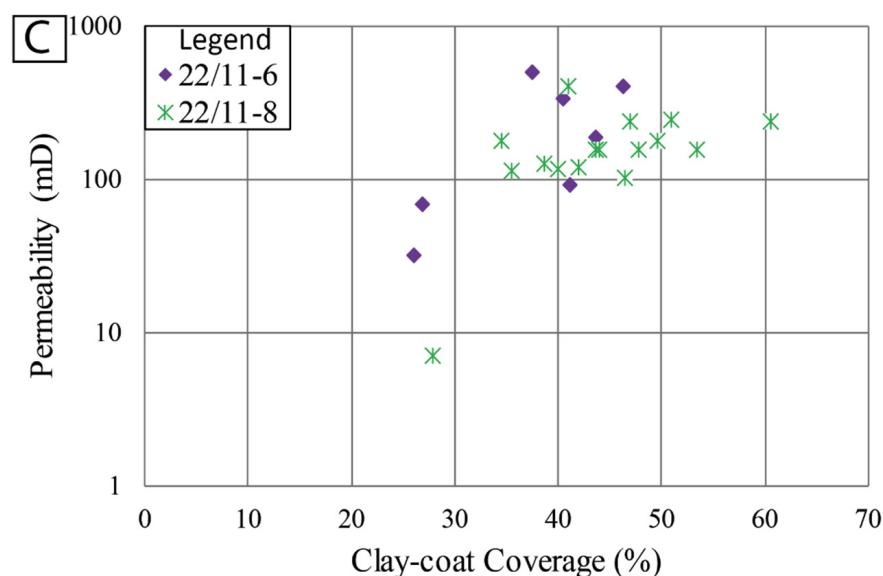


Figure 14. Role of grain-coating clays coverage on quartz cement and reservoir properties. (A) Plot of quartz cement volume against clay-coating coverage. (B) Plot of porosity against clay-coating coverage. (C) Plot of permeability against clay-coating coverage.

4.2. Controls on Porosity and Permeability Evolution of the Forties Sandstone Member

Porosity and permeability of the Forties Sandstone Member in the studied Nelson field is strongly controlled by primary depositional characteristics (e.g., grain size) and diagenetic alterations, which include mechanical compaction, formation of grain-coating chlorite and illite/illite-smectite, and cementation by quartz and carbonates (Figures 11 and 14). Sandstone samples from well 22/11-6 have larger grain size (and thus better porosity and permeability) than those from well 22/11-8 (Figure 11A,B).

Mechanical compaction is the main driver for porosity loss in samples from 22/11-8 (Figure 13), probably due to relatively higher mica content (average 3%) compared with those from 22/11-6, which have lower mica content (average < 1%). The mica grains bend around detrital grains, thereby enhancing porosity reduction due to compaction.

Pervasive cementation by ferroan and non-ferroan calcites, siderite, and dolomite (up to 15% in total) in samples from 22/11-6, notably those in close proximity to sandstone-mudstone contacts, induced substantial porosity reduction, where the cements might result in the compartmentalization of the reservoir by forming diagenetic baffles to fluid flow [68,69]. However, carbonate cements are less developed in 22/11-8. Thus, more porosity is lost due to carbonate cementation in 22/11-6 than in 22/11-8 (Figure 13).

The formation of grain-coating clays has significantly inhibited quartz cementation and preserved reservoir porosity and permeability in the sandstones. Grain-coating chlorite and illite, which were mainly formed from transformation of smectite, emplaced during the sediment dewatering process (Figure 6B,C) or inherited from continental, transitional or marine/shelf environments, were more developed in samples from 22/11-8 than in those from 22/11-6, resulting in clay-coating coverage of up to 61% and 46%, respectively. This is presumably because samples from 22/11-8 were buried deeper (2583–2608 m true vertical depth subsea (TVDSS) and thus experienced higher temperature for the formation of chlorite and illite compared to those from 22/11-6 (2206–2219 m TVDSS).

4.3. Suitability of the Forties Sandstone Member for Carbon Capture and Storage

As hydrocarbon production attains mature stage in almost all major oil and gas fields of the axial Forties Fan system [32], the Forties Sandstone Member can be a potential site for geologic carbon capture and storage (CCS). Reservoir porosity and permeability have been identified as key controls on the efficiency and effectiveness of CO₂ injection into the subsurface geological formations for both CO₂ storage and enhanced hydrocarbon

recovery. This is because low-porosity and low-permeability are often influenced by high volume of clay mineral and ductile grains, poor sorting, quartz cementation, and carbonate cements [16]. Geologic CO₂ storage, which mainly involves injecting CO₂ into deep, depleted hydrocarbon reservoirs, is considered to be the most effective method for long-term storage of large quantities of CO₂ [70,71]. Physical and solubility trapping, which involve trapping of CO₂ in structural and stratigraphic traps and dissolution of CO₂ into the pore water (respectively), are the most common geologic CO₂ storage mechanisms [72,73]. More recently, however, mineral trapping, involving carbonation of CO₂ to form calcite and dolomite, with Ca²⁺ and Mg²⁺ as key elements required for the process, are considered as the safest and most stable storage mechanism [74]. In addition, an experimental study by [75] simulating mineral trapping in anorthite-free arkosic sandstones using CaCl₂-rich formation water has precipitated calcite and kaolinite, suggesting that saline pore waters rich in CaCl₂, NaCl, KCl, and MgCl₂ are crucial for mineral trapping of CO₂. During the experiments, calcite and kaolinite precipitated, whereas albite and K-feldspar partly dissolved.

Consequently, characterized by good reservoir porosity and permeability, effective seal (Sele claystones), and an anticlinal closure (e.g., the Forties-Montrose High), the Forties Sandstone Member could be an ideal candidate for physical trapping. Additionally, the sandstones highly saline pore waters [76] and their arkosic composition (Figure 3) make them excellent potential sites for mineral trapping.

However, during CO₂ injection and storage, unstable minerals such as plagioclase, K-feldspar, kaolinite, illite, smectite, and chlorite are most susceptible to alteration due to CO₂-rock interaction [77]. The Forties Sandstone Member is composed predominantly of sub-rounded to rounded quartz (39.3%), plagioclase (5.8%), feldspar grains (16.9%), with clay minerals (5.3%), and carbonate cements (1.8%). The sandstones are poorly- to moderately well-sorted, grain sizes of 0.12 to 0.36 mm, with generally homogeneous structure and high porosity (23.9%). The high porosity is due to low degree of cementation, resulting in low tensile strength. The most susceptible minerals to alteration in the Forties Sandstone form a major proportion of the rock (>20% in total). While carbonate cements and chlorite can be subjected to dissolution during CO₂ injection and storage, smectite and kaolinite may be susceptible to adsorption, causing swelling or dewatering [77,78]. The dissolution of carbonate cements, feldspar, and chlorite can potentially increase the permeability of the sandstone by an order of magnitude. Nevertheless, the interplay between dissolution (e.g., feldspar, carbonates, and chlorite) and swelling (e.g., smectite, kaolinite, and illite) will favor dissolution due to the high feldspar content, opening pore volume during dissolution and enhancing an increase in permeability. Therefore, the geomechanical strength of the sandstone needs to be investigated as it determines how much (and at what pressure) CO₂ to be injected and the conditions required to be maintained to preserve borehole integrity.

5. Conclusions

Depositional characteristics (e.g., grain size) and diagenesis were the main controls on RQ of the Forties submarine channel sandstones. Sandstones with medium grain size have formed better RQ than those with finer grain size.

Diagenesis has played a vital role in RQ evolution of the Forties Sandstone Member. Overall, mechanical compaction is the main driver for porosity loss in the sandstones than cementation. Mechanical compaction was intense in sandstones with higher mica content, resulting in porosity deterioration due to compaction.

Grain-coating chlorite, illite-smectite, and illite were mainly sourced from detrital smectite, which was mainly emplaced during sediment dewatering process and/or was inherited from continental, transitional, or marine/shelf environments.

Grain-coating clays have preserved RQ by preventing quartz cementation, and >40% clay-coating coverage is required to significantly inhibit quartz cementation in the sandstones.

Pore-filling, diagenetic chlorite, illite, and kaolinite have had a detrimental effect on RQ of the sandstones, by blocking pore throats and reducing intergranular porosity. Pore-filling clays, as low as 10%, have impacted negatively on reservoir quality of the sandstones.

Sandstones pervasively cemented by carbonate cements (i.e., calcite, siderite, and dolomite) have caused porosity reduction due to cementation and might have contributed to the formation of compartmentalized reservoir by developing diagenetic baffles to fluid flow.

Author Contributions: A.M.B.: Conceptualization, data curation, investigation, formal analysis, funding acquisition, core sampling, methodology, software, writing (original draft), writing (review and editing); S.J.J.: supervision, resources, validation, and writing (review and editing); J.G.: supervision, resources, validation, and writing (review and editing); K.A.-R.: resources, validation, and writing (review and editing). All authors have read and agreed to the published version of the manuscript.

Funding: Petroleum Technology Development Fund (PTDF), Nigeria. Award number: PTDF/ED/PHD/BAM/1103/17.

Data Availability Statement: The data used to support the findings of this study are included within the article.

Conflicts of Interest: The Authors wish to state that they do not have any conflict of interests to declare.

References

1. Marchand, A.M.E.; Apps, G.; Li, W.; Rotzien, J.R. Depositional Processes and Impact on Reservoir Quality in Deepwater Paleogene Reservoirs, US Gulf of Mexico. *AAPG Bull.* **2015**, *99*, 1635–1648. [[CrossRef](#)]
2. Bell, D.; Kane, I.A.; Pontén, A.S.M.; Flint, S.S.; Hodgson, D.M.; Barrett, B.J. Spatial Variability in Depositional Reservoir Quality of Deep-Water Channel-Fill and Lobe Deposits. *Mar. Pet. Geol.* **2018**, *98*, 97–115. [[CrossRef](#)]
3. Huang, Y.; Kane, I.A.; Zhao, Y. Effects of Sedimentary Processes and Diagenesis on Reservoir Quality of Submarine Lobes of the Huangliu Formation in the Yinggehai Basin, China. *Mar. Pet. Geol.* **2020**, *120*, 104526. [[CrossRef](#)]
4. Porten, K.W.; Kane, I.A.; Warchoř, M.J.; Southern, S.J. A Sedimentological Process-Based Approach To Depositional Reservoir Quality of Deep-Marine Sandstones: An Example From the Springar Formation, Northwestern Vøring Basin, Norwegian Sea. *J. Sediment. Res.* **2016**, *86*, 1269–1286. [[CrossRef](#)]
5. Morad, S.; Al-Ramadan, K.; Ketzer, J.M.; De Ros, L.F. The Impact of Diagenesis on the Heterogeneity of Sandstone Reservoirs: A Review of the Role of Depositional Facies and Sequence Stratigraphy. *AAPG Bull.* **2010**, *94*, 1267–1309. [[CrossRef](#)]
6. Al-Ramadan, K.; Morad, S.; Norton, A.K.; Hulver, M. Linking Diagenesis and Porosity Preservation versus Destruction to Sequence Stratigraphy of Gas Condensate Reservoir Sandstones; the Jauf Formation (Lower to Middle Devonian), Eastern Saudi Arabia. *Link. Diagenesis Seq. Stratigr.* **2012**, *45*, 297e336. [[CrossRef](#)]
7. Oluwadebi, A.G.; Taylor, K.G.; Dowey, P.J. Diagenetic Controls on the Reservoir Quality of the Tight Gas Collyhurst Sandstone Formation, Lower Permian, East Irish Sea Basin, United Kingdom. *Sediment. Geol.* **2018**, *371*, 55–74. [[CrossRef](#)]
8. Barshep, D.V.; Worden, R.H. Reservoir Quality of Upper Jurassic Corallian Sandstones, Weald Basin, UK. *Geosciences* **2021**, *11*, 446. [[CrossRef](#)]
9. Al-Ramadan, K.; Franks, S.G.; Al-Shammari, S.; Rees, A.; Koeshidayatullah, A.; Abu-Khamsin, S. Depositional and Diagenetic Barriers, Baffles and Conduits: Permian—Carboniferous Unayzah Reservoir, Nuayyim Field, Central Saudi Arabia. *J. Pet. Geol.* **2017**, *40*, 85–103. [[CrossRef](#)]
10. Al-Ramadan, K. Illitization of Smectite in Sandstones: The Permian Unayzah Reservoir, Saudi Arabia. *Arab. J. Sci. Eng.* **2014**, *39*, 407–412. [[CrossRef](#)]
11. Al-Ramadan, K. The Role of Diagenesis at Unconformities of the Paleozoic Siliciclastic Succession of Central Saudi Arabia: Implications for Reservoir Quality. *Arab. J. Geosci.* **2021**, *14*, 484. [[CrossRef](#)]
12. Wilson, M.D.; Stanton, P.T. Diagenetic Mechanisms of Porosity and Permeability Reduction and Enhancement. In *Reservoir Quality Assessment and Prediction in Clastic Rocks*; Society for Sedimentary Geology: Tulsa, OK, USA, 1994; pp. 59–118. [[CrossRef](#)]
13. Worden, R.H.; Armitage, P.J.; Butcher, A.R.; Churchill, J.M.; Csoma, A.E.; Hollis, C.; Lander, R.H.; Omma, J.E. (Eds.) Petroleum Reservoir Quality Prediction: Overview and Contrasting Approaches from Sandstone and Carbonate Communities. In *Geological Society Special Publication*; Geological Society: London, UK, 2018; Volume 435, pp. 1–31.
14. Kupecz, J.A.; Gluyas, J.; Bloch, S. Reservoir Quality Prediction in Sandstones and Carbonates: An Overview. *AAPG Mem.* **1997**, vii–xxiv. Available online: <https://archives.datapages.com/data/specpubs/memoir69/data/a193/001/vii.htm> (accessed on 26 April 2022).
15. Bloch, S. Empirical Prediction of Porosity and Permeability in Sandstones. *Am. Assoc. Pet. Geol. Bull.* **1991**, *75*, 1145–1160. [[CrossRef](#)]

16. Xia, C.; Wilkinson, M. The Geological Risks of Exploring for a CO₂ Storage Reservoir. *Int. J. Greenh. Gas. Control.* **2017**, *63*, 272–280. [[CrossRef](#)]
17. Porten, K.W.; Warchoł, M.J.; Kane, I.A. Formation of Detrital Clay Grain Coats by Dewatering of Deep-Water Sands and Significance for Reservoir Quality. *J. Sediment. Res.* **2019**, *89*, 1231–1249. [[CrossRef](#)]
18. Blatt, H. Diagenetic Processes in Sandstones. *Soc. Econ. Paleontol. Mineral.* **1979**, *26*, 141–157. [[CrossRef](#)]
19. McBride, E.F. Quartz Cement in Sandstones: A Review. *Earth Sci. Rev.* **1989**, *26*, 69–112. [[CrossRef](#)]
20. Walderhaug, O. Precipitation Rates for Quartz Cement in Sandstones Determined by Fluid-Inclusion Microthermometry and Temperature–History Modeling. *J. Sediment. Res. Sediment. Petrol. Process.* **1994**, *64*, 324–333. [[CrossRef](#)]
21. Walderhaug, O.; Lander, R.H.; Bjørkum, P.A.; Oelkers, E.H.; Bjørlykke, K.; Nadeau, P.H. Modelling Quartz Cementation and Porosity in Reservoir Sandstones: Examples from the Norwegian Continental Shelf. *Quartz Cem. Sandstones* **2000**, *29*, 39–49. [[CrossRef](#)]
22. Ajdukiewicz, J.M.; Larese, R.E. How Clay Grain Coats Inhibit Quartz Cement and Preserve Porosity in Deeply Buried Sandstones: Observations and Experiments. *AAPG Bull.* **2012**, *96*, 2091–2119. [[CrossRef](#)]
23. Anjos, S.M.C.; De Ros, L.F.; Silva, C.M.A. Chlorite Authigenesis and Porosity Preservation in the Upper Cretaceous Marine Sandstones of the Santos Basin, Offshore Eastern Brazil. In *Clay Mineral Cements in Sandstones*; Worden, R.H., Morad, S., Eds.; International Association of Sedimentologists Special Publications: Oxford, UK, 2003; pp. 289–316.
24. Bloch, S.; Lander, R.H.; Bonnell, L. Anomalously High Porosity and Permeability in Deeply Buried Sandstone Reservoirs: Origin and Predictability. *AAPG Bull.* **2002**, *86*, 301–328. [[CrossRef](#)]
25. Busch, B.; Hilgers, C.; Adelman, D. Reservoir Quality Controls on Rotliegend Fluvio-Aeolian Wells in Germany and The Netherlands, Southern Permian Basin—Impact of Grain Coatings and Cements. *Mar. Pet. Geol.* **2020**, *112*, 104075. [[CrossRef](#)]
26. Ehrenberg, S.N. Preservation of Anomalously High Porosity in Deeply Buried Sandstones by Grain-Coating Chlorite: Examples from the Norwegian Continental Shelf. *AAPG Bull.* **1993**, *77*, 1260–1286.
27. Stricker, S.; Jones, S.J. Enhanced Porosity Preservation by Pore Fluid Overpressure and Chlorite Grain Coatings in the Triassic Skagerrak, Central Graben, North Sea, UK. *Geol. Soc. Spec. Publ.* **2018**, *435*, 321–341. [[CrossRef](#)]
28. Hansen, H.N.; Løvstad, K.; Lageat, G.; Clerc, S.; Jahren, J. Chlorite Coating Patterns and Reservoir Quality in Deep Marine Depositional Systems—Example from the Cretaceous Agat Formation, Northern North Sea, Norway. *Basin Res.* **2021**, *33*, 2725–2744. [[CrossRef](#)]
29. Bello, A.M.; Jones, S.; Gluyas, J.; Acikalin, S.; Cartigny, M. Role Played by Clay Content in Controlling Reservoir Quality of Submarine Fan System, Forties Sandstone Member, Central Graben, North Sea. *Mar. Pet. Geol.* **2021**, *128*, 105058. [[CrossRef](#)]
30. Dowey, P.J.; Hodgson, D.M.; Worden, R.H. Pre-Requisites, Processes, and Prediction of Chlorite Grain Coatings in Petroleum Reservoirs: A Review of Subsurface Examples. *Mar. Pet. Geol.* **2012**, *32*, 63–75. [[CrossRef](#)]
31. Worden, R.H.; Griffiths, J.; Wooldridge, L.J.; Utley, J.E.P.; Lawan, A.Y.; Muhammed, D.D.; Simon, N.; Armitage, P.J. Chlorite in Sandstones. *Earth-Sci. Rev.* **2020**, *204*, 103105. [[CrossRef](#)]
32. Hempton, M.; Marshall, J.; Sadler, S.; Hogg, N.; Charles, R.; Harvey, C. Turbidite Reservoirs of the Sele Formation, Central North Sea: Geological Challenges for Improving Production. *Pet. Geol. Conf. Proc.* **2005**, *6*, 449–459. [[CrossRef](#)]
33. Bowman, M.B.J. Cenozoic. In *Petroleum Geology of the North Sea*; Glennie, K.W., Ed.; Wiley: Hoboken, NJ, USA, 1998; pp. 350–375.
34. Vining, B.A.; Ioannides, N.S.; Pickering, K.T. Stratigraphic Relationships of Some Tertiary Lowstand Depositional Systems in the Central North Sea. In *Petroleum Geology Conference Proceedings*; Parker, J.R., Ed.; Geological Society: London, UK, 1993; Volume 4, pp. 17–29.
35. Collins, J.; Kenyon-Roberts, S.; Cullen, B.; White, J.; Bordas-Le Floch, N.; Downey, J. Arran Field: A Complex Heterolithic Reservoir on the Margins of the Forties Fan System. *Geol. Soc. Spec. Publ.* **2015**, *403*, 185–217. [[CrossRef](#)]
36. Jones, D.W.; Large, S.; McQueen, A.; Helmi, A. Reservoir Geology of the Paleocene Forties Sandstone Member in the Fram Discovery, UK Central North Sea. *Geol. Soc. Spec. Publ.* **2015**, *403*, 219–246. [[CrossRef](#)]
37. Jennette, D.C.; Garfield, T.R.; Mohrig, D.C.; Cayley, G.T. The Interaction of Shelf Accommodation, Sediment Supply and Sea Level in Controlling the Facies, Architecture and Sequence Stacking Patterns of the Tay and Forties/Sele Basin-Floor Fans, Central North Sea. In *Deep-Water Reservoirs of the World*; Weimer, P., Ed.; SEPM Society for Sedimentary Geology: Tulsa, OK, USA, 2000; Volume 20, ISBN 978-0-9836097-0-4.
38. Den Hartog Jager, D.; Giles, M.R.; Griffiths, G.R. Evolution of Paleogene Submarine Fans of the North Sea in Space and Time. *Pet. Geol. Conf. Proc.* **1993**, *4*, 59–71. [[CrossRef](#)]
39. Davis, C.; Haughton, P.; McCaffrey, W.; Scott, E.; Hogg, N.; Kitching, D. Character and Distribution of Hybrid Sediment Gravity Flow Deposits from the Outer Forties Fan, Palaeocene Central North Sea, UKCS. *Mar. Pet. Geol.* **2009**, *26*, 1919–1939. [[CrossRef](#)]
40. Charles, R.; Ryzhikov, K. Merganser Field: Managing Subsurface Uncertainty during the Development of a Salt Diapir Field in the UK Central North Sea. *Geol. Soc. Lond. Spec. Publ.* **2015**, *403*, 261–298. [[CrossRef](#)]
41. Scott, E.D.; Gelin, F.; Jolley, S.J.; Leenaarts, E.; Sadler, S.P.; Elsinger, R.J. Sedimentological Control of Fluid Flow in Deep Marine Turbidite Reservoirs: Pierce Field, UK Central North Sea. *Geol. Soc. Spec. Publ.* **2010**, *347*, 113–132. [[CrossRef](#)]
42. Whyatt, M.; Bowen, J.M.; Rhodes, D.N. The Nelson Field: A Successful Application of a Development Geoseismic Model in North Sea Exploration. *Geol. Soc. Spec. Publ.* **1992**, *67*, 283–305. [[CrossRef](#)]
43. Deegan, C.E.; Scull, B.J. *A Proposed Standard Lithostratigraphic Nomenclature for the Mesozoic of the Central and Northern North Sea*; Institute of Geological Sciences Report: London, UK, 1977; pp. 1–24.

44. Knox, R.W.O.; Holloway, S. Paleogene of the Central and Northern North Sea. In *Lithostratigraphic nomenclature of the UK North Sea*; Knox, R.W.O., Cowdey, W.G., Eds.; British Geological Survey: Nottingham, UK, 1992; p. 206.
45. Neal, J.E. A Summary of Paleogene Sequence Stratigraphy in Northwest Europe and the North Sea. In *Correlation of the Early Paleogene in Northwest Europe*; Knox, R.W.O., Corfield, R.M., Dunay, R.E., Eds.; Geological Society Special Publications: London, UK, 1996; pp. 15–42.
46. Eldrett, J.; Tripsanas, E.; Davis, C.; Mckie, T.; Vieira, M.; Osterloff, P.; Sandison, T. Sedimentological Evolution of Sele Formation Deep-Marine Depositional Systems of the Central North Sea. *Tert. Deep-Mar. Reserv. North Sea Reserv. North Sea* **2015**, *403*, 63–98. [[CrossRef](#)]
47. Kilhams, B.; Morton, A.; Borella, R.; Wilkins, A.; Hurst, A. Understanding the Provenance and Reservoir Quality of the Sele Formation Sandstones of the UK Central Graben Utilizing Detrital Garnet Suites. *Geol. Soc. Spec. Publ.* **2014**, *386*, 129–142. [[CrossRef](#)]
48. Mudge, D.C.; Copestake, P. A Revised Lower Palaeogene Lithostratigraphy for the Outer Moray Firth. *Mar. Pet. Geol.* **1993**, *9*, 53–69. [[CrossRef](#)]
49. Kunka, J.M.; Williams, G.; Cullen, B.; Boyd-Gorst, J.; Dyer, G.R.; Garnham, J.A.; Warnock, A.; Wardell, J.; Davis, A.; Lynes, P. The Nelson Field, Blocks 22/11, 22/61, 22/7, 22/12a, UK North Sea. In *Geological Society Memoir*; Gluyas, J.G., Hichens, H.M., Eds.; Geological Society: London, UK, 2003; Volume 20, pp. 617–646.
50. Dutton, S.P.; Hutton, M.E.; Ambrose, W.A.; Childers, A.T.; Loucks, R.G. Preservation of Reservoir Quality by Chlorite Coats in Deep Tuscaloosa Sandstones, Central Louisiana, USA. *Gulf Coast Assoc. Geol. Soc.* **2018**, *7*, 46–58.
51. Lundegard, P.D. Sandstone Porosity Loss—A 'big Picture' View of the Importance of Compaction. *J. Sediment. Petrol.* **1992**, *62*, 250–260. [[CrossRef](#)]
52. Paxton, S.T.; Szabo, J.O.; Ajdukiewicz, J.M.; Klimentidis, R.E. Construction of an Intergranular Volume Compaction Curve for Evaluating and Predicting Compaction and Porosity Loss in Rigid-Grain Sandstone Reservoirs. *AAPG Bull.* **2002**, *86*, 2047–2067. [[CrossRef](#)]
53. Pryor, W.A. Permeability-Porosity Patterns and Variations in Some Holocene Sand Bodies. *AAPG Bull.* **1973**, *57*, 162–189. [[CrossRef](#)]
54. Allsop, T. Early Compaction History of Marine Siliciclastic Sediments. PhD Thesis, Durham University, Durham, UK, 1994.
55. Folk, R.L. *Petrology of Sedimentary Rocks*; Hemphill Publishing Company: Austin, TX, USA, 1980.
56. Lien, T.; Midtbø, R.E.; Martinsen, O.J. Depositional Facies and Reservoir Quality of Deep-Marine Sandstones in the Norwegian Sea. *Nor. Geol. Tidsskr.* **2006**, *86*, 71–92.
57. Lowe, D.R. Sediment Gravity Flows: II. Depositional Models with Special Reference to the Deposits of High-Density Turbidity Currents. *J. Sediment. Petrol.* **1982**, *52*, 279–297. [[CrossRef](#)]
58. Stanley, D.J. Welded Slump-Graded Sand Couples: Evidence for Slide Generated Turbidity Currents. *Geo-Mar. Lett.* **1982**, *2*, 149–155. [[CrossRef](#)]
59. Górska, M.E. Verification of Gravity-Flow Models: Case Study from the Lower Eocene Sediments (Tylmanowa Site, SE Poland). *Baltica* **2019**, *32*, 30–50. [[CrossRef](#)]
60. Dutton, S.P.; Scott Hamlin, H.; Folk, R.L.; Clift, S.J. Early Siderite Cementation as a Control on Reservoir Quality in Submarine Fan Sandstones, Sonora Canyon Gas Play, Val Verde Basin, Texas. In *Siliciclastic Diagenesis and Fluid Flow: Concepts and Applications*; Crossey, L.J., Loucks, R., Totten, M.W., Scholle, P.A., Eds.; SEPM Society for Sedimentary Geology: Tulsa, OK, USA, 1996; Volume 55, ISBN 978-1-56576-178-0.
61. Berner, R.A. A New Geochemical Classification of Sedimentary Environments. *J. Sediment. Petrol.* **1981**, *51*, 359–366. [[CrossRef](#)]
62. Berner, R.A. Sedimentary Pyrite Formation. *Am. J. Sci.* **1970**, *268*, 1–23. [[CrossRef](#)]
63. Burley, S.D.; Kantorowicz, J.D.; Waugh, B. *Clastic Diagenesis*; Geological Society Special Publications: London, UK, 1985; Volume 18, pp. 189–226. [[CrossRef](#)]
64. Worden, R.H.; Morad, S. Clay Minerals in Sandstones: Controls on Formation, Distribution and Evolution. In *Clay Mineral Cements in Sandstones*; Blackwell Publishing Ltd.: Oxford, UK, 2003; Volume 34, pp. 1–41.
65. Marfil, R.; Delgado, A.; Rossi, C.; Iglesia, A.L.; Ramseyer, K. Origin and Diagenetic Evolution of Kaolin in Reservoir Sandstones and Associated Shales of the Jurassic and Cretaceous, Salam Field, Western Desert (Egypt). *Clay Miner. Cem. Sandstones* **2003**, *34*, 317–342. [[CrossRef](#)]
66. Stewart, R.N.T.; Haszeldine, R.S.; Fallick, A.E.; Wilkinson, M.; Macaulay, C.I. Regional Distribution of Diagenetic Carbonate Cement in Palaeocene Deepwater Sandstones: North Sea. *Clay Miner.* **2000**, *35*, 119–133. [[CrossRef](#)]
67. Ehrenberg, S.N. Relationship between Diagenesis and Reservoir Quality in Sandstones of the Garn Formation, Haltenbanken, Mid-Norwegian Continental Shelf. *Am. Assoc. Pet. Geol. Bull.* **1990**, *74*, 1538–1558. [[CrossRef](#)]
68. Al-Ramadan, K.; Morad, S.; Proust, J.N.; Al-Aasm, I. Distribution of Diagenetic Alterations in Siliciclastic Shoreface Deposits within a Sequence Stratigraphic Framework: Evidence from the Upper Jurassic, Boulonnais, NW France. *J. Sediment. Res.* **2005**, *75*, 943–959. [[CrossRef](#)]
69. Ketzer, J.M.; Holz, M.; Morad, S.; Al-Aasm, I.S. Sequence Stratigraphic Distribution of Diagenetic Alterations in Coal-Bearing, Paralic Sandstones: Evidence from the Rio Bonito Formation (Early Permian), Southern Brazil. *Sedimentology* **2003**, *50*, 855–877. [[CrossRef](#)]

70. Celia, M.A.; Nordbotten, J.M. Practical Modeling Approaches for Geological Storage of Carbon Dioxide. *Ground Water* **2009**, *47*, 627–638. [[CrossRef](#)]
71. Myer, L. Global Status of Geologic CO₂ Storage Technology Development. *United States Carbon Sequestrat. Counc. Rep. July* **2011**, *2011*, 26.
72. Li, Y.; Pang, Z. Capacity and Suitability Assessment of Deep Saline Aquifers for CO₂ Sequestration in the Bohai Bay Basin, East China. *Environ. Earth Sci.* **2016**, *75*, 1–15. [[CrossRef](#)]
73. Shukla, R.; Ranjith, P.; Haque, A.; Choi, X. A Review of Studies on CO₂ Sequestration and Caprock Integrity. *Fuel* **2010**, *89*, 2651–2664. [[CrossRef](#)]
74. Yang, L.; Xu, T.; Feng, G.; Liu, K.; Tian, H.; Peng, B.; Wang, C. CO₂-Induced Geochemical Reactions in Heterogeneous Sandstone and Potential Conditions Causing the Tight Cementation. *Appl. Geochem.* **2017**, *80*, 14–23. [[CrossRef](#)]
75. Yanzhong, W.; Nianmin, Z.; Xu, C.; Yingchang, C.; Guanghui, Y.; Gluyas, J.G.; Miruo, L. Geologic CO₂ Storage in Arkosic Sandstones with CaCl₂-Rich Formation Water. *Chem. Geol.* **2020**, *558*, 119867. [[CrossRef](#)]
76. Crawford, R.; Littlefair, R.W.; Affleck, L.G. The Arbroath and Montrose Fields, Blocks 22/17, 18, UK North Sea. *Geol. Soc. Mem.* **1991**, *14*, 211–217. [[CrossRef](#)]
77. Allen, M.J.; Faulkner, D.R.; Worden, R.H.; Rice-Birchall, E.; Katirtsidis, N.; Utley, J.E.P. Geomechanical and Petrographic Assessment of a CO₂ Storage Site: Application to the Acorn CO₂ Storage Site, Offshore United Kingdom. *Int. J. Greenh. Gas. Control.* **2020**, *94*, 102923. [[CrossRef](#)]
78. Busch, A.; Alles, S.; Gensterblum, Y.; Prinz, D.; Dewhurst, D.; Raven, M.; Stanjek, H.; Krooss, B. Carbon Dioxide Storage Potential of Shales. *Int. J. Greenh. Gas. Control.* **2008**, *2*, 297–308. [[CrossRef](#)]